Model-independent investigation of rare semileptonic $b \to u l \bar{\nu}_l$ decay processes

Suchismita Sahoo, Atasi Ray, and Rukmani Mohanta
School of Physics, University of Hyderabad, Hyderabad 500046, India
(Received 15 August 2017; published 20 December 2017)

Motivated by the recent observation of lepton universality violation in the flavor changing charged current transitions $b \to c l \bar{\nu}_l$, we intend to scrutinize the lepton nonuniversality effects in rare semileptonic B meson decays involving the quark-level transitions $b \to u l \bar{\nu}_l$. In this regard, we envisage the model-independent approach and consider the generalized effective Lagrangian in the presence of new physics and constrain the new parameters by using the experimental branching fractions of $B_u^+ \to l^+ \nu_l$ and $B^- \to \pi^0 \mu^- \bar{\nu}_\mu$ processes, in which $l = e, \mu, \tau$. We then estimate the branching ratios and forward-backward asymmetries of $B_{(s)} \to P(V) l \bar{\nu}_l$ processes, in which $P(= K, \pi, \eta^{(\prime)})$ denotes the pseudoscalar meson and $V(= K^*, \rho)$ is the vector meson. We also find out various lepton nonuniversality parameters in these processes in the presence of new physics.

DOI: 10.1103/PhysRevD.96.115017

I. INTRODUCTION

In recent times, flavor physics has become quite interesting as several deviations at the level of $(2-4)\sigma$ have persistently been observed in semileptonic B decays. Specifically, the LHCb experiment has observed several anomalies in the rare semileptonic B decays driven by the flavor changing neutral current $b \to s$ transitions. The most leading ones are the observation of 3.7σ deviation in the angular observables P_5' [1,2], the decay rate of the $\bar{B} \to \bar{K}^{(*)} \mu^+ \mu^-$ mode [3], and also the 3σ [4] discrepancy in the decay rate of the $B_s \to \phi \mu^+ \mu^-$ process in the low q^2 region. Besides these anomalies, recently, LHCb and B factories have observed the violation of lepton flavor universality in $B \to D^{(*)} l \bar{\nu}_l$ and $B \to K^{(*)} l^+ l^-$ processes, which comprises some additional tension. The lepton nonuniversality (LNU) parameter (R_K), defined as the ratio of the branching fractions of $B^+ \to K^+ \mu^+ \mu^-$ over $B^+ \to K^+ e^+ e^-$ and its measured value in the low $q^2 \in [1, 6]$ region [5]

$$R_K^{\rm Expt} = \frac{{\rm BR}(B^+ \to K^+ \mu^+ \mu^-)}{{\rm BR}(B^+ \to K^+ e^+ e^-)} = 0.745^{+0.090}_{-0.074} \pm 0.036, \quad (1)$$

has 2.6σ deviation from the corresponding standard model (SM) result $R_K^{\rm SM} = 1.0003 \pm 0.0001$ [6]. In addition, very recently, the LHCb Collaboration has also reported a discrepancy of 2.2σ in R_{K^*} [7],

$$R_{K^*}^{\rm Expt} = \frac{{\rm BR}(B \to K^* \mu^+ \mu^-)}{{\rm BR}(B \to K^* e^+ e^-)} = 0.660^{+0.110}_{-0.070} \pm 0.024, \quad (2)$$

from the corresponding SM prediction $R_{K^*}^{\rm SM} = 0.92 \pm 0.02$ [8] in the $q^2 \in [0.045, 1.1]$ GeV^2 bin, and a 2.4σ discrepancy [7],

$$R_{K^*}^{\rm Expt} = 0.685^{+0.113}_{-0.069} \pm 0.047, \quad (3)$$

has been found in the $q^2 \in [1.1, 6]$ GeV^2 region from its SM predicted value $R_{K^*}^{\rm SM} = 1.00 \pm 0.01$ [8].

Analogously, in the charged current transition processes mediated through $b \to c \tau \bar{\nu}_\tau$, LHCb as well as both the B factories Belle and *BABAR* have measured the LNU parameter $R_{D^{(*)}}$ in $B \to D^{(*)} l \bar{\nu}_l$ decay processes, and the measured values [9–11]

$$R_D^{\rm Expt} = \frac{{\rm BR}(B \to D \tau \nu_l)}{{\rm BR}(B \to D l \nu_l)} = 0.397 \pm 0.040 \pm 0.028, \quad (4)$$

$$R_{D^*}^{\rm Expt} = \frac{{\rm BR}(B \to D^* \tau \nu_l)}{{\rm BR}(B \to D^* l \nu_l)} = 0.316 \pm 0.016 \pm 0.010 \quad (5)$$

have, respectively, 1.9σ and 3.3σ deviation from the corresponding SM predictions [12,13]

$$R_D^{\rm SM} = 0.300 \pm 0.008, \qquad R_{D^*}^{\rm SM} = 0.252 \pm 0.003. \quad (6)$$

In this context, we wish to explore the possibility of observing LNU parameters and other asymmetries in the rare semileptonic $b \to u l \bar{\nu}_l$ decay processes, in order to corroborate the observed results on lepton nonuniversality.

In the SM, the $V - A$ current structure of the weak interactions describes various charged current interactions for all three generations of quarks and leptons to high precision. However, the recent experimental data indicate that among all the leptonic and semileptonic decays of B mesons the decay processes involving the third generation of fermions in the final state are comparatively less precise than the first two generations. The coupling of the third-generation fermions to the electroweak gauge sector is relatively stronger due to the heavier mass of the tau lepton and thus more sensitive to new physics (NP) which could modify the $V-A$ structure of the SM. The decays with third-generation fermions in the final state are sensitive to non-SM contributions arising from the violation of LFU; hence, these processes could be ideally suited for probing the NP signature. In this respect, the study of $B \to (\pi, \rho, \eta^{(\prime)}) l\bar{\nu}_l$ and $B_s \to K^{(*)} l\bar{\nu}_l$ charged current processes, involving the quark-level transitions $b \to u$, would be quite interesting for testing the lepton flavor nonuniversality. In this paper, we adopt the model-independent approach to analyze the effect of NP in the rare semileptonic $b \to ul\bar{\nu}_l$ decay processes. For this purpose, we consider the generalized effective Lagrangian, including the possible new parameters allowed by Lorentz invariance. We constrain the new coefficients by using the experimental data on the branching fractions of $B_u^+ \to l^+\nu_l$ processes. We then compute the branching ratios, forward-backward asymmetries, and various LNU parameters of semileptonic $B \to (\pi, \rho, \eta^{(\prime)}) l\nu_l$ and $B_s \to K^{(*)} l\nu_l$ processes. Although these processes have been extensively studied in the literature [14–24], in the context of various new physics models and also in a model-independent way, the search for lepton nonuniversality parameters is not being explored.

The outline of the paper is as follows. In Sec. II, we describe the most general effective Lagrangian responsible for the $b \to ul\bar{\nu}_l$ processes. We also show the constraints on the new parameters by using the branching ratios of $B_u^+ \to l^+\bar{\nu}_l$ processes. The constraint on new physics couplings from the $B^- \to \pi^0\mu^-\bar{\mu}_\nu$ process is presented in Sec. III. We also estimate the branching ratios, forward-backward asymmetries, and the LNU parameters of the $B \to Pl\bar{\nu}_l$ processes, in which $P(= K, \pi, \eta^{(\prime)})$ represents the pseudoscalar meson, in Sec. III. In Sec. IV, we study the rare semileptonic $B \to Vl\bar{\nu}_l$ processes, in which $V(= K^*, \rho)$ denotes the vector meson. Our findings are summarized in Sec. V.

II. GENERAL EFFECTIVE LAGRANGIAN FOR $b \to ul\bar{\nu}_l$ TRANSITIONS

The most general effective Lagrangian for the $b \to ul\bar{\nu}_l$ process is given by [25]

$$\begin{aligned}\mathcal{L}_{\rm eff} = -\frac{4G_F}{\sqrt{2}} V_{ub}\{&(1+V_L)\bar{l}_L\gamma_\mu\nu_L\bar{u}_L\gamma^\mu b_L \\ &+ V_R\bar{l}_L\gamma_\mu\nu_L\bar{u}_R\gamma^\mu b_R + S_L\bar{l}_R\nu_L\bar{u}_R b_L + S_R\bar{l}_R\nu_L\bar{u}_L b_R \\ &+ T_L\bar{l}_R\sigma_{\mu\nu}\nu_L\bar{u}_R\sigma^{\mu\nu}b_L\} + \text{H.c.},\end{aligned} \tag{7}$$

where G_F is the Fermi constant, V_{ub} is the Cabibbo-Kobayashi-Maskawa (CKM) matrix element, and $q_{L(R)} = L(R)q$ are the chiral quark fields with $L(R) = (1 \mp \gamma_5)/2$ as the projection operator. Here, $V_{L,R}$, $S_{L,R}$, and T_L are the vector, scalar, and tensor new physics couplings associated with the left-handed neutrinos, which are zero in the SM. The constraints on the new coefficients obtained from the leptonic $B_u^+ \to l^+\nu_l$ processes are discussed in the subsection below.

A. Constraints on new couplings from rare leptonic $B_u^+ \to l^+\nu_l$ processes

The rare leptonic $B_u^+ \to l^+\nu_l$ processes are mediated by the quark-level transitions $b \to u$ and are theoretically very clean. The only nonperturbative quantity involved in these processes is the decay constant of the B_u meson. Including the new coefficients from Eq. (7), the branching ratios of $B_u^+ \to l^+\nu_l$ processes in the presence of NP are given by [26]

$$\begin{aligned}\text{BR}(B_u^+ \to l^+\nu_l) &= \frac{G_F^2 M_{B_u} m_l^2}{8\pi}\left(1-\frac{m_l^2}{M_{B_u}^2}\right)^2 f_{B_u}^2 |V_{ub}|^2 \tau_{B_u^+} \\ &\times \left|(1+V_L-V_R) - \frac{M_{B_u}^2}{m_l(m_b+m_u)}(S_L-S_R)\right|^2,\end{aligned} \tag{8}$$

where $M_{B_u}(f_{B_u})$ is the mass (decay constant) of the B_u meson and m_l is the lepton mass. In our analysis, all the particle masses and the lifetime of the B_u^+ meson are taken from Ref. [27]. The decay constant of the B_u meson is taken as $f_{B_u} = 190.5(4.2)$ MeV [28], and for the CKM matrix element, we use the Wolfenstein parametrization with the values $A = 0.811 \pm 0.026$, $\lambda = 0.22506 \pm 0.00050$, $\bar{\rho} = 0.124^{+0.019}_{-0.018}$, and $\bar{\eta} = 0.356 \pm 0.011$ [27]. Using these values, the obtained branching fractions of $B_u^+ \to l^+\nu_l$ processes in the SM are given as

$$\begin{aligned}\text{BR}(B_u^+ \to e^+\nu_e)|^{\rm SM} &= (8.9 \pm 0.23) \times 10^{-12}, \\ \text{BR}(B_u^+ \to \mu^+\nu_\mu)|^{\rm SM} &= (3.83 \pm 0.1) \times 10^{-7}, \\ \text{BR}(B_u^+ \to \tau^+\nu_\tau)|^{\rm SM} &= (8.48 \pm 0.28) \times 10^{-5},\end{aligned} \tag{9}$$

and the corresponding experimental values are [27]

$$\begin{aligned}\text{BR}(B_u^+ \to e^+\nu_e)|^{\rm Expt} &< 9.8 \times 10^{-7}, \\ \text{BR}(B_u^+ \to \mu^+\nu_\mu)|^{\rm Expt} &< 1.0 \times 10^{-6}, \\ \text{BR}(B_u^+ \to \tau^+\nu_\tau)|^{\rm Expt} &= (1.09 \pm 0.24) \times 10^{-4}.\end{aligned} \tag{10}$$

Since $B_u^+ \to l^+\nu_l$ processes do not receive any contribution from tensor coupling, we ignore the effect of the tensor operator in this work. In our analysis, we consider the new coefficients $V_{L,R}$ and $S_{L,R}$ as complex. For simplicity, we consider the presence of only one coefficient at a time and constrain its real and imaginary parts by comparing the predicted SM branching fractions of $B_u^+ \to l^+\nu_l$ processes with the corresponding experimental results. For $B_u^+ \to \tau^+\nu_\tau$, we compare with the 1σ range of observed data. In Fig. 1, we show the constraints on the real and

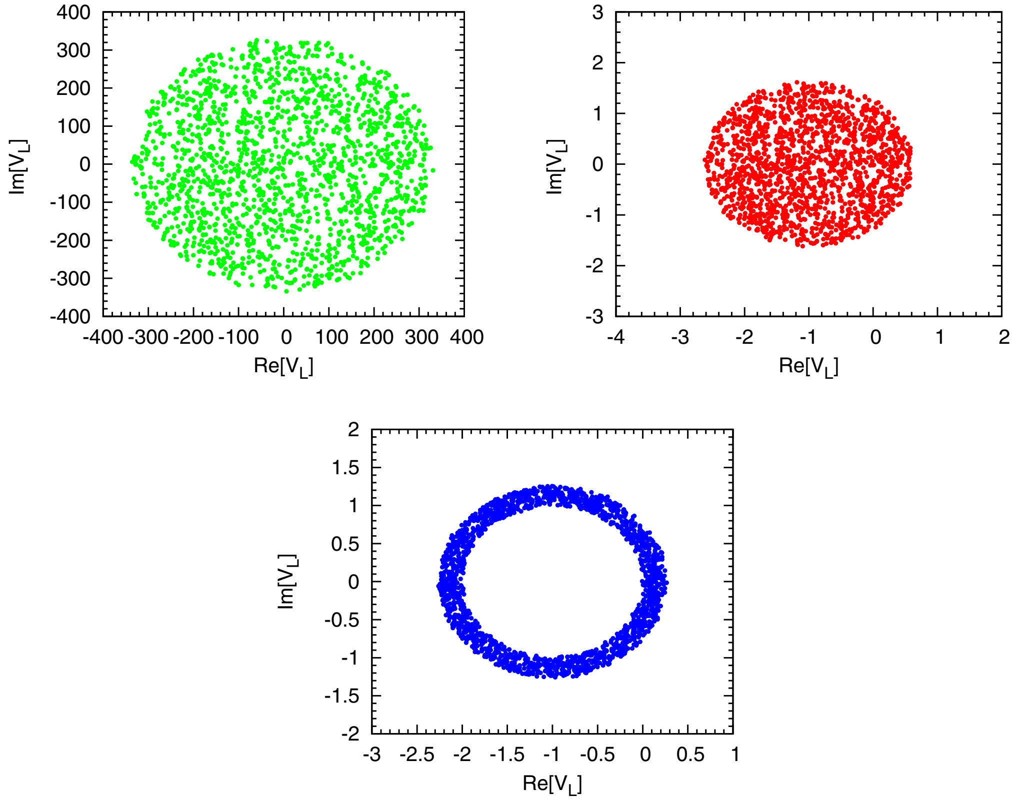

FIG. 1. Constraint on the real and imaginary parts of the V_L parameter obtained from $B_u^+ \to e^+\nu_e$ (top-left panel), $B_u^+ \to \mu^+\nu_\mu$ (top-right panel), and $B_u^+ \to \tau^+\nu_\tau$ (bottom panel).

imaginary parts of the V_L coefficient obtained from the $B_u^+ \to e^+\nu_e$ (top-left panel), $B_u^+ \to \mu^+\nu_\mu$ (top-right panel), and $B_u^+ \to \tau^+\nu_\tau$ (bottom panel) processes. Analogously, the allowed ranges of the real and imaginary parts of the S_L coefficient derived from the $B_u^+ \to e^+\nu_e$ (top-left panel), $B_u^+ \to \mu^+\nu_\mu$ (top-right panel), and $B_u^+ \to \tau^+\nu_\tau$ (bottom panel) processes are shown in Fig. 2. The constraint on the imaginary part of the $V_R(S_R)$ coefficient is the same as the $V_L(S_L)$ coefficient, and the corresponding real part is related by $\mathrm{Re}[V_R](\mathrm{Re}[S_R]) = -\mathrm{Re}[V_L](\mathrm{Re}[S_L])$. It should be noted that the bounds obtained from the $B_u^+ \to e^+\nu_e(\mu^+\nu_\mu)$ process are comparatively weak as only the upper limits on the branching ratios of these processes exist. Furthermore, the bounds on new coefficients obtained from the $B_u^+ \to e^+\nu_e$ process are too weak to make reasonable predictions for the observables associated with $b \to ue^+\nu_e$ decay modes. Therefore, we only present the results for semileptonic B decays with $\mu(\tau)$ in the final state.

III. $B \to Pl\bar{\nu}_l$ PROCESSES

In this section, we discuss the rare $B \to Pl\bar{\nu}_l$ processes, in which $P = \pi, K, \eta^{(\prime)}$. The matrix elements of various hadronic currents between the initial B meson and the final pseudoscalar meson P can be parametrized in terms of two form factors F_0 and F_1 [29,30] as

$$\langle P(k)|\bar{u}\gamma_\mu b|B(p_B)\rangle = F_1(q^2)\left[(p_B+k)_\mu - \frac{M_B^2 - M_P^2}{q^2}q_\mu\right] + F_0(q^2)\frac{M_B^2-M_P^2}{q^2}q_\mu, \tag{11}$$

where p_B and k are, respectively, the 4-momenta of the B and P mesons and $q = p_B - k$ is the momentum transfer. Now, using the above form factors, the double differential decay distribution of $B \to Pl\nu_l$ processes in terms of the helicity amplitudes H_0, H_t, and H_S is given by [30]

$$\begin{aligned}\frac{d\Gamma(B\to Pl\bar{\nu}_l)}{dq^2} &= \frac{G_F^2|V_{ub}|^2}{192\pi^3 M_B^3}q^2\sqrt{\lambda_P(q^2)}\left(1-\frac{m_l^2}{q^2}\right)^2 \\ &\times\left\{|1+V_L+V_R|^2\left[\left(1+\frac{m_l^2}{2q^2}\right)H_0^2+\frac{3}{2}\frac{m_l^2}{q^2}H_t^2\right]\right. \\ &+\frac{3}{2}|S_L+S_R|^2H_S^2+3\mathrm{Re}[(1+V_L+V_R) \\ &\left.\times(S_L^*+S_R^*)]\frac{m_l}{\sqrt{q^2}}H_SH_t\right\},\end{aligned}\tag{12}$$

where

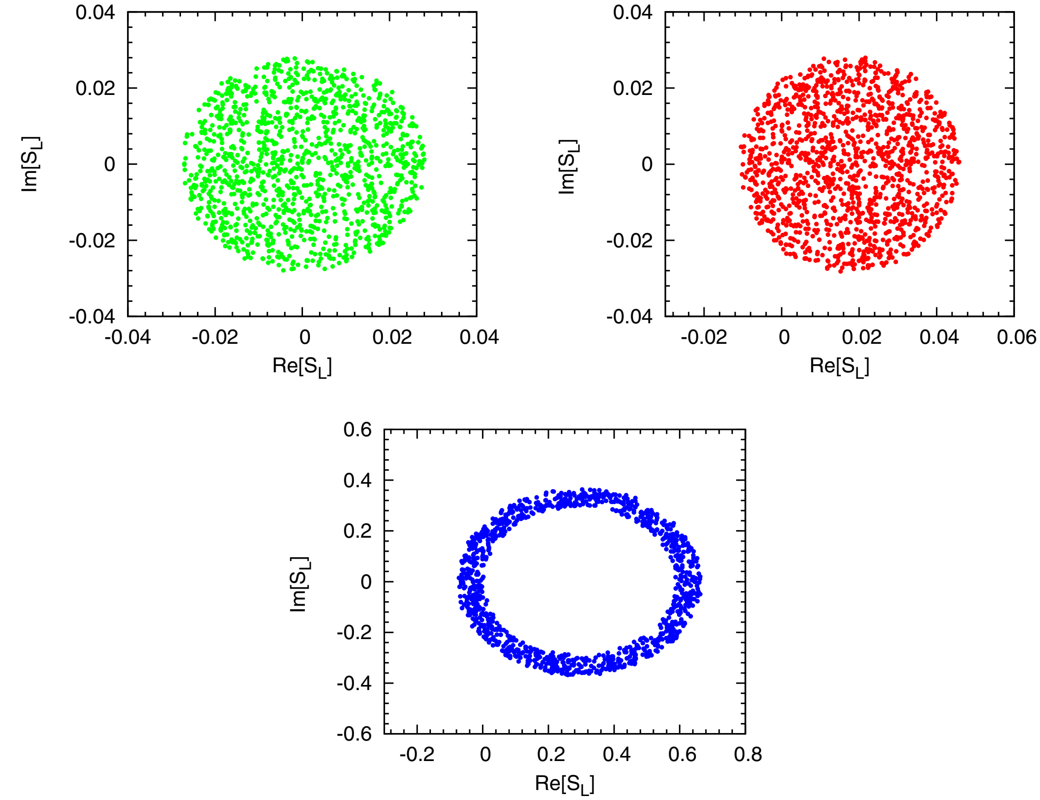

FIG. 2. Constraint on the real and imaginary parts of the S_L parameter obtained from $B_u^+ \to e^+\nu_e$ (top-left panel), $B_u^+ \to \mu^+\nu_\mu$ (top-right panel), and $B_u^+ \to \tau^+\nu_\tau$ (bottom panel).

$$\lambda_P = \lambda(M_B^2, M_P^2, q^2) \\ = M_B^4 + M_P^4 + q^4 - 2(M_B^2 M_P^2 + M_P^2 q^2 + M_B^2 q^2), \qquad (13)$$

and the helicity amplitudes $(H_{0,t,S})$ in terms of the form factors $(F_{0,1})$ are given as

$$H_0(q^2) = \sqrt{\frac{\lambda_P(q^2)}{q^2}} F_1(q^2),$$

$$H_t(q^2) = \frac{M_B^2 - M_P^2}{\sqrt{q^2}} F_0(q^2),$$

$$H_S(q^2) = \frac{M_B^2 - M_P^2}{m_b - m_u} F_0(q^2). \qquad (14)$$

Here, M_P is the mass of the P meson, and $m_b(m_u)$ is the mass of the $b(u)$ quark.

The lepton forward-backward asymmetry, which is an interesting observable to look for NP, is defined as

$$A_{FB}(q^2) = \frac{\int_0^1 \frac{d\Gamma}{dq^2 d\cos\theta} d\cos\theta - \int_{-1}^0 \frac{d\Gamma}{dq^2 d\cos\theta} d\cos\theta}{d\Gamma/dq^2}. \qquad (15)$$

Besides the branching ratio and forward-backward asymmetry, another important observable is the LNU ratio. Similar to $R_{D^{(*)}}$ observables, we define the LNU parameter for $B \to P l \nu_l$ processes as

$$R_P^{\tau\mu} = \frac{\mathrm{BR}(B \to P\tau\bar{\nu}_\tau)}{\mathrm{BR}(B \to P\mu\bar{\nu}_\mu)} \qquad (16)$$

in order to scrutinize the violation of lepton universality effect in $b \to u l \nu_l$ decays. In Ref. [13], the authors have studied the lepton universality violating ratio $\mathrm{BR}(B \to P\tau\bar{\nu}_\tau)/\mathrm{BR}(B \to P l \bar{\nu}_l)$, where $l = e, \mu$. Since the constraints on new coefficients obtained from the $B_u^+ \to e^+\nu_e$ process are too weak, it would not be possible to predict a reasonably constrained result for the $\mathrm{BR}(B \to P\tau\bar{\nu}_\tau)/\mathrm{BR}(B \to P e\bar{\nu}_e)$ ratio. Therefore, we only consider the $\mathrm{BR}(B \to P\tau\bar{\nu}_\tau)/\mathrm{BR}(B \to P\mu\bar{\nu}_\mu)$ parameter in our analysis.

To explore a few other observables that are sensitive to NP in the $b \to u l \bar{\nu}_l$ processes, we define the parameter $R_{PP'}^l$ as a ratio of branching fractions of $B \to P l^- \bar{\nu}_l$ to $B \to P' l^- \bar{\nu}_l$ processes,

$$R_{PP'}^l = \frac{\mathrm{BR}(B \to P l^- \bar{\nu}_l)}{\mathrm{BR}(B \to P' l^- \bar{\nu}_l)}. \qquad (17)$$

These processes differ only in the spectator quark content, and hence any deviation from the SM prediction, if observed, would hint toward the existence of NP.

Now that the stage has been set, we proceed to numerical analysis. We consider all the particle masses and the lifetime of B meson from Ref. [27]. To make predictions for the various observables or to extract information about potentially new short distance physics, one should have sufficient knowledge of the associated hadronic form factors. For the form factors of $\bar{B}_s \to K^+ l^- \bar{\nu}_l$ processes, we consider the perturbative QCD (PQCD) calculation [17,18] based on the k_T factorization [31] at next-to-leading order in α_s [32], which gives

$$F_1^{B_s\to K}(q^2) = F_1^{B_s\to K}(0)\left(\frac{1}{(1-q^2/M_{B_s}^2)} + \frac{a_1 q^2/M_{B_s}^2}{(1-q^2/M_{B_s}^2)(1-b_1 q^2/M_{B_s}^2)}\right),$$
$$F_0^{B_s\to K}(q^2) = \frac{F_0^{B_s\to K}(0)}{(1-a_0 q^2/M_{B_s}^2 + b_0 q^4/M_{B_s}^4)}, \tag{18}$$

where M_{B_s} is the mass of B_s meson and the values of the parameters $a_{0,1}$, $b_{0,1}$, and $F_{0,1}^{B_s\to K}$ are listed in Table I.

For $B \to \pi$ form factors, we use the light cone sum rule (LCSR) results as input for a z-series parametrization, which yield the q^2 shape in the whole semileptonic region of $B \to \pi l \nu_l$ processes. The q^2 dependence of the form factors is parametrized as [33]

$$F_1(q^2) = \frac{F_1(0)}{\left(1-\frac{q^2}{M_{B^*}2}\right)}\left\{1 + \sum_{k=1}^{N-1} b_k \left(z(q^2,t_0)^k - z(0,t_0)^k - (-1)^{N-k}\frac{k}{N}\left[z(q^2,t_0)^N - z(0,t_0)^N\right]\right)\right\},$$
$$F_0(q^2) = F_0(0)\left\{1 + \sum_{k=1}^{N} b_k^0 (z(q^2,t_0)^k - z(0,t_0)^k)\right\}, \tag{19}$$

where $N=2$ for the $F_1(q^2)$ form factor and $N=1$ for the $F_0(q^2)$ form factor. Here, the function $z(q^2,t_0)$ is defined as [34]

TABLE I. Numerical values of the $B_s \to K$ form factors in the PQCD approach [17].

Parameters	PQCD
$F_0(0)$	$0.26^{+0.04}_{-0.03} \pm 0.02$
a_0	$0.54 \pm 0.00 \pm 0.05$
b_0	$-0.15 \pm 0.00 \pm 0.00$
$F_1(0)$	$0.26 \pm 0.035 \pm 0.02$
a_1	$0.57 \pm 0.01 \pm 0.02$
b_1	$0.50 \pm 0.01 \pm 0.05$

$$z(q^2,t_0) = \frac{\sqrt{(M_B+M_\pi)^2 - q^2} - \sqrt{(M_B+M_\pi)^2 - t_0}}{\sqrt{(M_B+M_\pi)^2 - q^2} + \sqrt{(M_B+M_\pi)^2 - t_0}}, \tag{20}$$

where $t_0 = (M_B+M_\pi)^2 - 2\sqrt{M_B M_\pi}\sqrt{(M_B+M_\pi)^2 - q^2_{\min}}$ is the auxiliary parameter. Here, the values of various parameters involved are $F_1(0) = F_0(0) = 0.281 \pm 0.028$, $b_1 = -1.62 \pm 0.70$, and $b_1^0 = -3.98 \pm 0.97$ [33].

The $B^- \to \eta^{(\prime)} l^- \bar{\nu}_l$ processes are also mediated by the flavor changing charged current transitions $b \to u$. For the study of these processes, we use $SU(3)_F$ flavor symmetry to relate the form factors of $F_1^{B\to\eta^{(\prime)}}$ to $F_1^{B\to\pi}$. We choose the scheme as discussed in Refs. [35,36] and consider

$$|\eta\rangle = \cos\phi|\eta_q\rangle - \sin\phi|\eta_s\rangle,$$
$$|\eta'\rangle = \sin\phi|\eta_q\rangle + \cos\phi|\eta_s\rangle, \tag{21}$$

for the $\eta - \eta'$ mixing, where $|\eta_q\rangle = (u\bar{u} + d\bar{d})/\sqrt{2}$, $\eta_s = s\bar{s}$, and ϕ is the fitted mixing angle ($\phi = 39.3°$) [36]. With these input parameters in hand, we now proceed to discuss four different new physics scenarios and their effect on $b \to u l \nu_l$ processes.

A. Case A: Effect of V_L only

In this case, we assume that only the new V_L coefficient is present in addition to the SM contribution, in the effective Lagrangian (7). From Eq. (12), it should be noted that as the NP has the same structure as the SM the SM decay rate gets modified by the factor $|1+V_L|^2$. The constraints on the real and imaginary parts of the V_L coefficient for $b \to u\tau\bar{\nu}_\tau$ are obtained from the branching ratio of the $B_u^+ \to \tau^+\nu_\tau$ process as discussed in Sec. II. From the bottom panel of Fig. 1, one can notice that the constraint on V_L is $|V_L| \le 2.5$, obtained from the $B_u \to \tau\bar{\nu}_\tau$ process. In our analysis, we consider the values for real and imaginary parts of V_L, which give the maximum and minimum values of the branching ratio within the 1σ limit. Thus, imposing the extrema conditions, the allowed parameters are found as $(\mathrm{Re}[V_L], \mathrm{Im}[V_L])^{\max} = (0.130, 0.761)$ and $(\mathrm{Re}[V_L], \mathrm{Im}[V_L])^{\min} = (-0.929, 0.841)$. Since only the upper limit of $B_u \to \mu\bar{\nu}_\mu$ is known, it will not provide any strict bound on the new V_L coupling associated with $b \to s\mu\bar{\nu}_\mu$ transition. Comparing the SM predicted value $\mathrm{BR}(B^- \to \pi^0\mu^-\bar{\nu}_\mu)^{\mathrm{SM}} = (7.15 \pm 0.55) \times 10^{-5}$ with the 1σ range of the corresponding measured value $\mathrm{BR}(B^- \to \pi^0\mu^-\bar{\nu}_\mu)^{\mathrm{Expt}} = (7.80 \pm 0.27) \times 10^{-5}$, we obtain the maximum and minimum values of the V_L parameter as $(\mathrm{Re}[V_L], \mathrm{Im}[V_L])^{\max} = (-0.233, 0.769)$ and $(\mathrm{Re}[V_L], \mathrm{Im}[V_L])^{\min} = (-0.833, 0.968)$. The corresponding allowed parameter space is shown in the left panel of Fig. 3.

Using the allowed constrained values, we show the plots for the variation of branching fractions of various

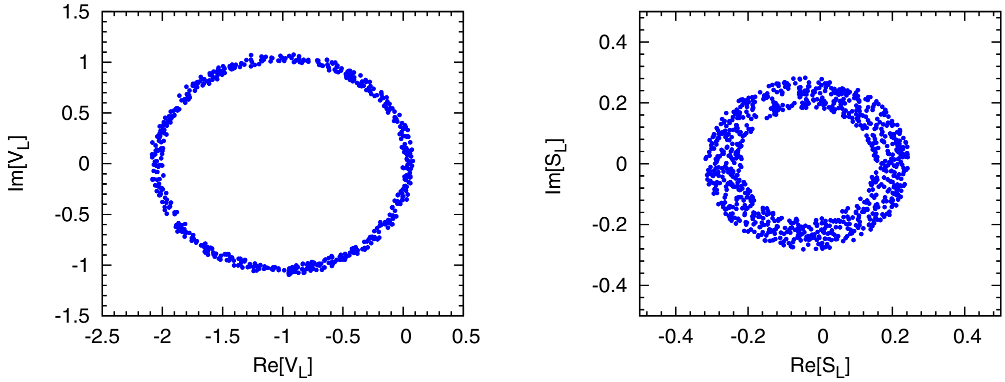

FIG. 3. Constraint on the real and imaginary parts of the V_L (left panel) and S_L (right panel) parameters obtained from the $B_u^- \to \pi^0 \mu \bar{\nu}_\mu$ process.

$B \to P\mu^-\bar{\nu}_\mu$ processes with respect to q^2 in Fig. 4, both in the SM and in the NP scenario. Here, the plot for the $\bar{B}_s \to K^+\mu^-\bar{\nu}_\mu$ process is represented in the top-left panel, the top-right panel is for the branching ratio of $\bar{B}^0 \to \pi^+\mu^-\bar{\nu}_\mu$, the bottom-left plot is for the $B^- \to \eta\mu^-\bar{\nu}_\mu$ process, and the branching ratio of the $B^- \to \eta'\mu^-\bar{\nu}_\mu$ process is presented in the bottom-right panel. In these figures, the red bands are due to the contribution coming from the V_L new physics parameter in addition to the SM, and the blue dashed lines are due to the SM. The green bands are the corresponding SM theoretical uncertainties, which arise due to the uncertainties in the SM input parameters such as CKM elements and form factors. Analogous plots for the variation of the branching ratios of $\bar{B}_s \to K^+\tau^-\bar{\nu}_\tau$ (top-left panel), $\bar{B}^0 \to \pi^+\tau^-\bar{\nu}_\tau$ (top-right panel), $B^- \to \eta\tau^-\bar{\nu}_\tau$ (bottom-left panel), and $B^- \to \eta'\tau^-\bar{\nu}_\tau$ (bottom-right panel) processes are shown in Fig. 5. The integrated values of the branching ratios for these processes are given in Table II. Because of the inclusion of the new V_L coefficient, we found a certain deviation in the branching ratios of $B \to P\tau\bar{\nu}_\tau$ processes

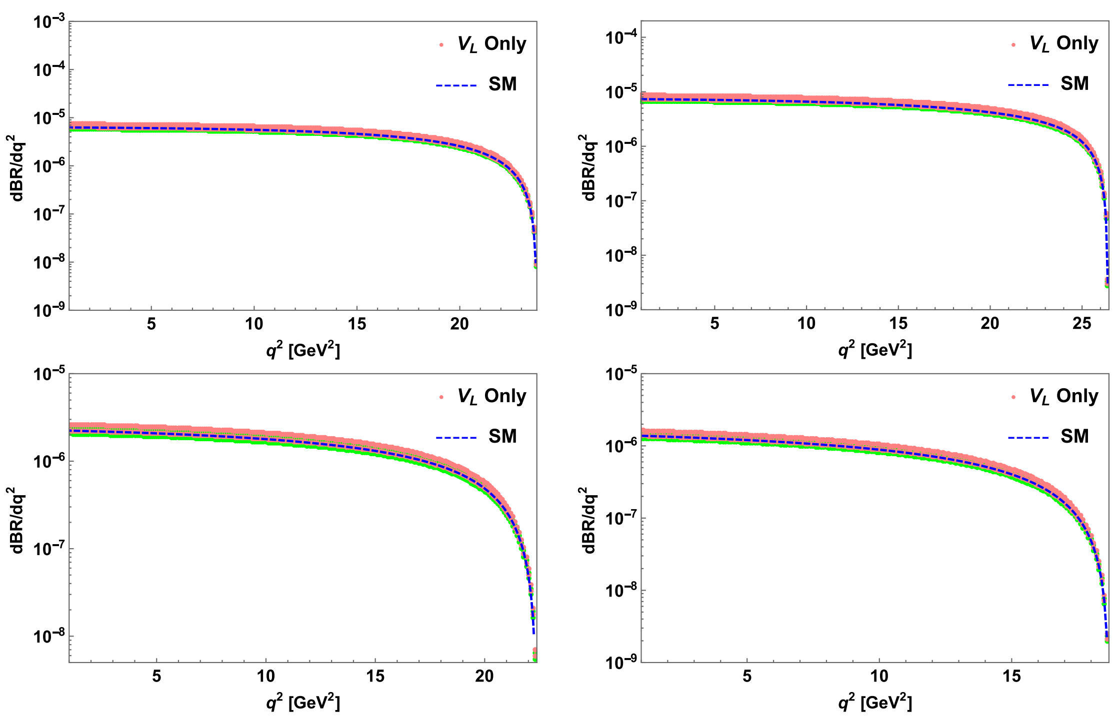

FIG. 4. The plots for the q^2 variation of the branching ratios of $\bar{B}_s \to K^+\mu^-\bar{\nu}_\mu$ (top-left panel), $\bar{B}^0 \to \pi^+\mu^-\nu_\mu$ (top-right panel), $B^- \to \eta\mu^-\bar{\nu}_\mu$ (bottom-left panel), and $B^- \to \eta'\mu^-\bar{\nu}_\mu$ (bottom-right panel) processes for the NP contribution coming from only V_L coupling. Here, the red bands represent the contributions due to the V_L coupling. The blue dashed lines are for the SM contribution, and the green bands are due to the contributions coming from the theoretical uncertainties.

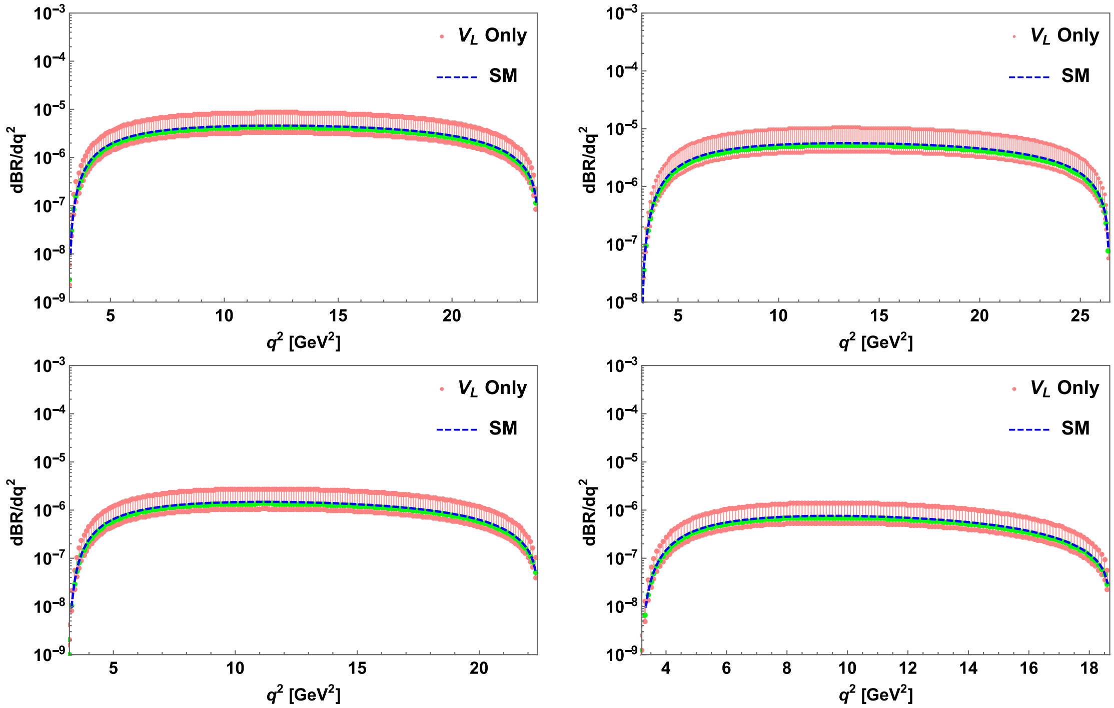

FIG. 5. The plots for the q^2 variation of the branching ratios of $\bar{B}_s \to K^+\tau^-\bar{\nu}_\tau$ (top-left panel), $\bar{B}^0 \to \pi^+\tau^-\nu_\tau$ (top-right panel), $B^- \to \eta\tau^-\bar{\nu}_\tau$ (bottom-left panel), and $B^- \to \eta'\tau^-\bar{\nu}_\tau$ (bottom-right panel) processes for the NP contribution due to V_L coupling.

from the SM values, whereas the deviation in the branching ratios of $B \to P\mu\bar{\nu}_\mu$ processes are relatively small. Our predicted results for $B \to (\pi, \eta^{(\prime)})l\nu_l$ processes are consistent with the existing experimental data [27]:

$$\begin{aligned} \mathrm{BR}(B^+ \to \eta l^+\nu_l)^{\mathrm{Expt}} &= (3.8 \pm 0.6) \times 10^{-5}, \\ \mathrm{BR}(B^0 \to \pi^- l^+\nu_l)^{\mathrm{Expt}} &= (1.45 \pm 0.05) \times 10^{-4}, \\ \mathrm{BR}(B^+ \to \eta' l^+\nu_l)^{\mathrm{Expt}} &= (2.3 \pm 0.8) \times 10^{-5}, \\ \mathrm{BR}(B^0 \to \pi^-\tau^+\nu_\tau)^{\mathrm{Expt}} &< 2.5 \times 10^{-4}. \end{aligned} \tag{22}$$

Since the V_L contribution has the same structure as the SM, the forward-backward asymmetry parameter of $B \to P\mu^-\bar{\nu}_\mu(\tau^-\bar{\nu}_\tau)$ processes does not deviate from their SM values, and the corresponding integrated values (integrated over the whole q^2 range) are presented in Table II. In Fig. 6, we show the plots for the LNU parameters of $\bar{B}_{(s)} \to Pl\bar{\nu}_l$ processes, $R_K^{\tau\mu}$ (top-left panel), $R_\pi^{\tau\mu}$ (top-right panel), $R_\eta^{\tau\mu}$ (bottom-left panel), and $R_{\eta'}^{\tau\mu}$ (bottom-right panel). Including only the V_L coupling, we also compute the $R_{\pi K}^l$, $R_{\pi\eta}^l$, and $R_{\pi\eta'}^l$ parameters; however, no deviation has been found from their corresponding SM result. The numerical values of these parameters are listed in Table III.

B. Case B: Effect of V_R only

Here, we consider the effect of only the V_R coefficient in addition to the SM contribution. The constraints obtained on the real and imaginary parts of the V_R coupling from the $B_u \to \tau\nu$ process are related to that of V_L as $\mathrm{Re}[V_R] = -\mathrm{Re}[V_L]$ and $\mathrm{Im}[V_R] = \mathrm{Im}[V_L]$, and thus the allowed parameter space for V_R is the same as that of V_L with a sign flip for the real parts. The minimum and maximum values of the V_R parameters are obtained using the extrema conditions as $(\mathrm{Re}[V_R], \mathrm{Im}[V_R])^{\max} = (-0.242, -0.561)$ and $(\mathrm{Re}[V_R], \mathrm{Im}[V_R])^{\min} = (0.259, -0.406)$. However, the constraints on V_R obtained from $B^- \to \pi^0\mu^-\bar{\nu}_\mu$ for the $b \to u\mu\bar{\nu}_\mu$ transition are same as V_L. Thus, the predicted branching ratios for $B \to P\mu\bar{\nu}_\mu$ processes in the presence of V_R coupling are the same as those with V_L coupling. Using the allowed values of the couplings, the plots for the branching ratios of $\bar{B}_s \to K^+\tau^-\bar{\nu}_\tau$ (top-left panel), $\bar{B}^0 \to \pi^+\tau^-\bar{\nu}_\tau$ (top-right panel), $B^- \to \eta\tau^-\bar{\nu}_\tau$ (bottom-left panel), and $B^- \to \eta'\tau^-\bar{\nu}_\tau$ (bottom-right panel) processes in the presence of V_R coupling are shown in Fig. 7. In these plots, the cyan bands are obtained by using the allowed parameter space of V_R. The predicted integrated values of branching ratios of these processes are listed in Table II. Like the previous case, the forward-backward asymmetry parameters are also not affected due to V_R coupling. In Fig. 8, we present the plots for the LNU parameters $R_K^{\tau\mu}(q^2)$ (top-left panel), $R_\pi^{\tau\mu}(q^2)$ (top-right panel), $R_\eta^{\tau\mu}(q^2)$ (bottom-left panel), and $R_{\eta'}^{\tau\mu}(q^2)$ (bottom-right panel). In the presence of V_R coupling, the parameters $R_{\pi K}^l, R_{\pi\eta^{(\prime)}}^l$ do not have any deviation from their corresponding SM predictions. In Table III, we present the numerical values of these parameters.

TABLE II. The predicted branching ratios and forward-backward asymmetries of $\bar{B}_{(s)} \to P l \bar{\nu}_l$ processes, in which $P = K, \pi, \eta^{(\prime)}$ and $l = \mu, \tau$ in the SM and in the presence of $V_{L,R}$ NP couplings.

Observables	Values in the SM	Values for V_L coupling	Values for V_R coupling
$\mathrm{BR}(\bar{B}_s \to K^+ \mu^- \bar{\nu}_\mu)$	$(1.03 \pm 0.082) \times 10^{-4}$	$(1.03 - 1.22) \times 10^{-4}$	$(1.03 - 1.22) \times 10^{-4}$
$\mathrm{BR}(\bar{B}_s \to K^+ \tau^- \bar{\nu}_\tau)$	$(6.7 \pm 0.536) \times 10^{-5}$	$(0.477 - 1.24) \times 10^{-4}$	$(0.6 - 1.17) \times 10^{-4}$
$\langle A_{FB}^\mu \rangle$	$(2.98 \pm 0.238) \times 10^{-3}$	2.98×10^{-3}	2.98×10^{-3}
$\langle A_{FB}^\tau \rangle$	0.275 ± 0.022	0.275	0.275
$\mathrm{BR}(\bar{B} \to \pi^+ \mu^- \bar{\nu}_\mu)$	$(1.35 \pm 0.1) \times 10^{-4}$	$(1.35 - 1.59) \times 10^{-4}$	$(1.35 - 1.59) \times 10^{-4}$
$\mathrm{BR}(\bar{B} \to \pi^+ \tau^- \bar{\nu}_\tau)$	$(9.4 \pm 0.752) \times 10^{-5}$	$(0.67 - 1.75) \times 10^{-4}$	$(0.824 - 1.62) \times 10^{-4}$
$\langle A_{FB}^\mu \rangle$	$(2.94 \pm 0.235) \times 10^{-3}$	2.94×10^{-3}	2.94×10^{-3}
$\langle A_{FB}^\tau \rangle$	(0.27 ± 0.021)	0.27	0.27
$\mathrm{BR}(B^- \to \eta \mu^- \bar{\nu}_\mu)$	$(3.143 \pm 0.25) \times 10^{-5}$	$(3.143 - 3.7) \times 10^{-5}$	$(3.143 - 3.7) \times 10^{-5}$
$\mathrm{BR}(B^- \to \eta \tau^- \bar{\nu}_\tau)$	$(1.96 \pm 0.16) \times 10^{-5}$	$(1.4 - 3.64) \times 10^{-5}$	$(1.75 - 3.43) \times 10^{-5}$
$\langle A_{FB}^\mu \rangle$	$(3.45 \pm 0.276) \times 10^{-3}$	3.45×10^{-3}	3.45×10^{-3}
$\langle A_{FB}^\tau \rangle$	(0.292 ± 0.023)	0.292	0.292
$\mathrm{BR}(B^- \to \eta' \mu^- \bar{\nu}_\mu)$	$(1.45 \pm 0.116) \times 10^{-5}$	$(1.45 - 1.7) \times 10^{-5}$	$(1.45 - 1.7) \times 10^{-5}$
$\mathrm{BR}(B^- \to \eta' \tau^- \bar{\nu}_\tau)$	$(7.81 \pm 0.06) \times 10^{-6}$	$(0.56 - 1.45) \times 10^{-5}$	$(0.695 - 1.37) \times 10^{-5}$
$\langle A_{FB}^\mu \rangle$	$(4.1 \pm 0.328) \times 10^{-3}$	4.1×10^{-3}	4.1×10^{-3}
$\langle A_{FB}^\tau \rangle$	(0.317 ± 0.026)	0.317	0.317

C. Case C: Effect of S_L only

In this subsection, we wish to see the effect of only S_L coupling on various observables associated with $B \to P l \bar{\nu}_l$ processes. For $b \to u \tau \nu$ transition, using the extrema conditions, we obtain the maxima and minima of S_L parameter as $(\mathrm{Re}[S_L], \mathrm{Im}[S_L])^{\max} = (-0.1063, -0.0063)$ and $(\mathrm{Re}[S_L], \mathrm{Im}[S_L])^{\min} = (0.5397, 0.0244)$, from the allowed parameter space in the bottom panel of Fig. 2.

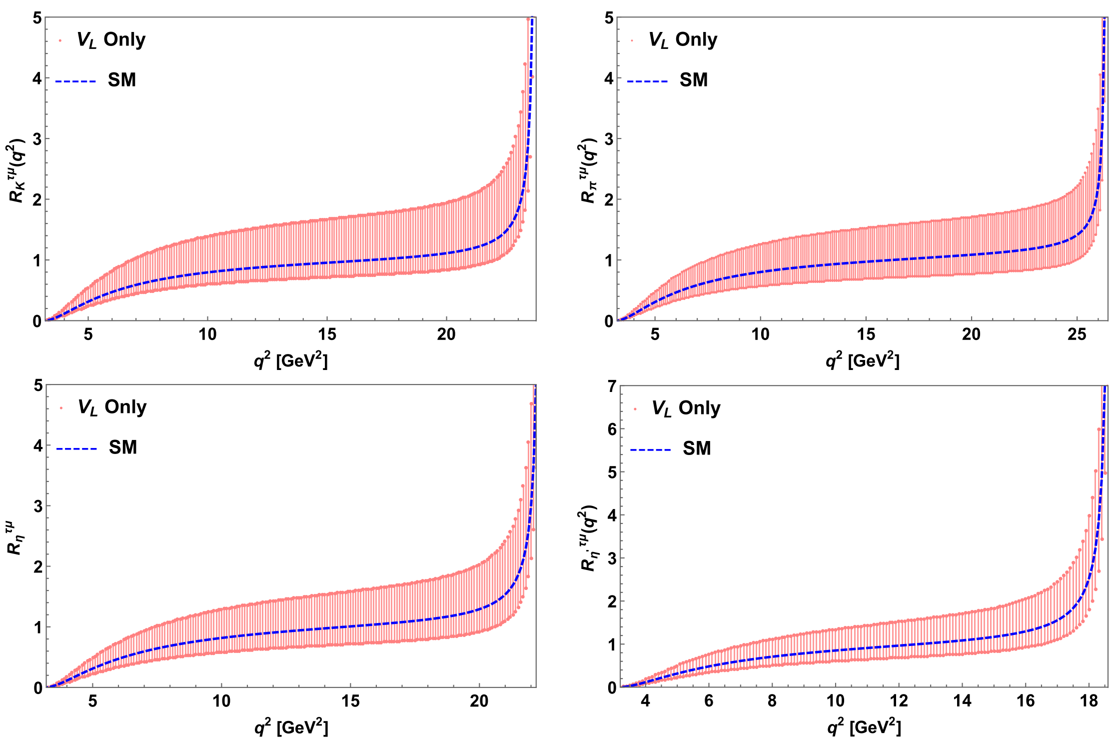

FIG. 6. The plots for the LNU parameters $R_K^{\tau\mu}(q^2)$ (top-left panel), $R_\pi^{\tau\mu}(q^2)$ (top-right panel), $R_\eta^{\tau\mu}(q^2)$ (bottom-left panel), and $R_{\eta'}^{\tau\mu}(q^2)$ (bottom-right panel) for the NP contribution due to V_L coupling.

TABLE III. The predicted values of various parameters ($R_P^{\tau\mu}$ and $R_{PP'}^{l}$) of $\bar{B}_{(s)} \to P l \bar{\nu}_l$ processes in the SM and in the presence of $V_{L,R}$ NP couplings.

Observables	Values in the SM	Values for V_L coupling	Values for V_R coupling
$R_K^{\tau\mu}$	0.649	0.46–1.02	0.489–1.13
$R_\pi^{\tau\mu}$	0.7	0.497–1.1	0.528–1.22
$R_\eta^{\tau\mu}$	0.624	0.45–0.982	0.47–1.09
$R_{\eta'}^{\tau\mu}$	0.54	0.385–0.85	0.408–0.946
$R_{\pi K}^{\mu}$	1.31	1.3–1.31	1.3–1.31
$R_{\pi\eta}^{\mu}$	4.3	4.3	4.3
$R_{\pi\eta'}^{\mu}$	9.3	9.3–9.35	9.3–9.35
$R_{\pi K}^{\tau}$	1.4	1.4–1.41	1.373–1.39
$R_{\pi\eta}^{\tau}$	4.8	4.785–4.808	4.709–4.723
$R_{\pi\eta'}^{\tau}$	12.0	11.96–12.1	11.82–11.86

Analogously, for $b \to u\mu\bar{\nu}_\mu$, the extrema values of S_L are found to be $(\mathrm{Re}[S_L], \mathrm{Im}[S_L])^{\max} = (-0.163, 0.252)$ and $(\mathrm{Re}[S_L], \mathrm{Im}[S_L])^{\min} = (0.017, 0.176)$, and the corresponding 1σ range of allowed parameter space is shown in the right panel of Fig. 3. Including the additional contributions from S_L coupling, the obtained branching ratios for various processes are listed in Table IV. It is observed that the branching ratios of $\bar{B}_{(s)} \to P^+\tau^-\bar{\nu}_\tau$ processes comparatively deviate more than the corresponding processes with the muon in the final state.

Figure 9 represents the q^2 variation of the forward-backward asymmetry of $\bar{B}_s \to K^+\mu^-\bar{\nu}_\mu$ (top-left panel), $\bar{B}^0 \to \pi^+\mu^-\bar{\nu}_\mu$ (top-right panel), $B^- \to \eta\mu^-\bar{\nu}_\mu$ (bottom-left panel), and $B^- \to \eta'\mu^-\bar{\nu}_\mu$ (bottom-right panel) processes for only S_L coupling. The corresponding plots for $\bar{B}_{(s)} \to P\tau\bar{\nu}_\tau$ processes are given in Fig. 10. Because of the additional S_L contribution, the forward-backward asymmetry parameters of these processes deviate significantly from SM. The corresponding integrated values are presented in Table IV. Figure 11 represents the plots for the LNU parameters $R_K^{\tau\mu}(q^2)$ (top-left panel), $R_\pi^{\tau\mu}(q^2)$ (top-right panel), $R_\eta^{\tau\mu}(q^2)$ (bottom-left panel), and $R_{\eta'}^{\tau\mu}(q^2)$ (bottom-right panel) versus q^2. The variation of $R_{\pi K}^{\tau}$ and $R_{\pi\eta^{(\prime)}}^{\tau}$ parameters with respect to q^2 are shown in Fig. 12. In Table V, we give the numerical values of these parameters.

D. Case D: Effect of S_R only

Here, we perform an analysis of $B \to Pl^-\bar{\nu}_l$ processes with the additional S_R coupling. As discussed in Sec. II, the real part of S_R coupling differs from the real part of S_L by a negative sign, while their imaginary parts are same. The minimum and maximum values of the S_R parameter are found as $(\mathrm{Re}[S_R], \mathrm{Im}[S_R])^{\max} = (0.003, 0.268)$ and $(\mathrm{Re}[S_R], \mathrm{Im}[S_R])^{\min} = (-0.54, -0.03)$ for the $b \to u\tau\bar{\nu}_\tau$ process. For $b \to u\mu\nu$, the constraints on S_R

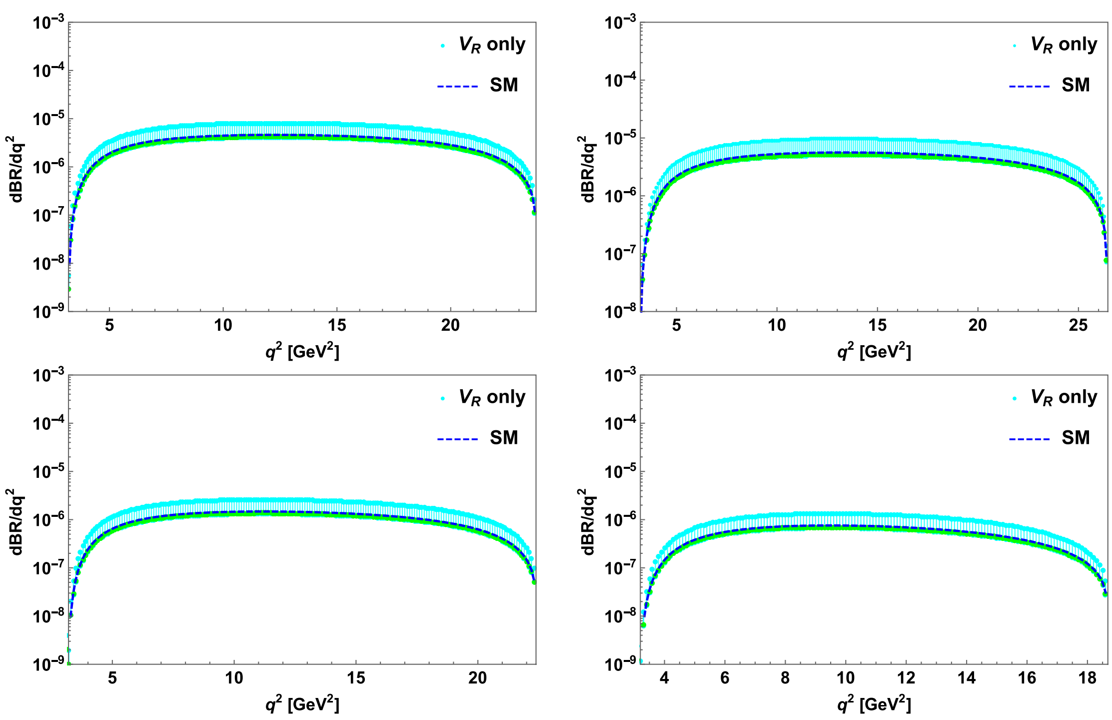

FIG. 7. The plots for the branching ratios of $B_s \to K^+\tau^-\bar{\nu}_\tau$ (top-left panel), $\bar{B}^0 \to \pi^+\tau^-\bar{\nu}_\tau$ (top-right panel), $B^- \to \eta\tau^-\bar{\nu}_\tau$ (bottom-left panel), and $B^- \to \eta'\tau^-\bar{\nu}_\tau$ (bottom-right panel) processes for the NP contribution of only V_R coupling. Here, the cyan bands are for the V_R NP coupling contributions.

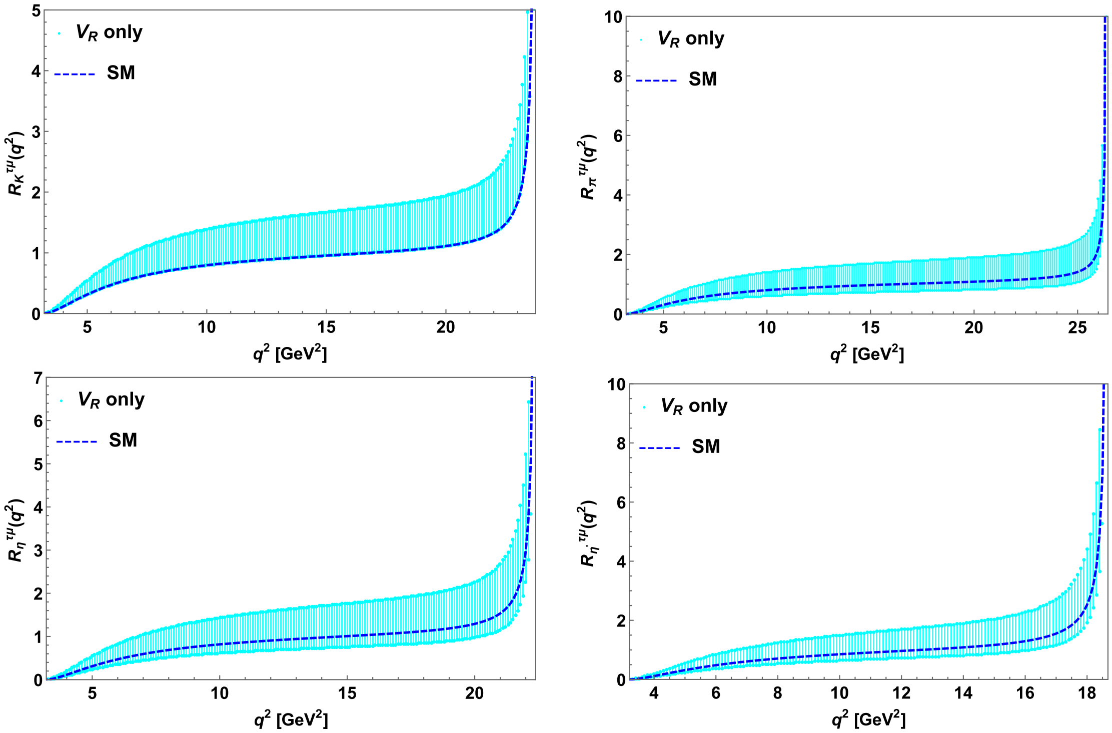

FIG. 8. The plots for the LNU parameters $R_K^{\tau\mu}(q^2)$ (top-left panel), $R_\pi^{\tau\mu}(q^2)$ (top-right panel), $R_\eta^{\tau\mu}(q^2)$ (bottom-left panel), and $R_{\eta'}^{\tau\mu}(q^2)$ (bottom-right panel).

couplings are the same as S_L. Using these values, the q^2 variation of the forward-backward asymmetries for $B^- \to P^0\tau^-\bar{\nu}_\tau$ processes is shown in Fig. 13. The branching ratios and forward-backward asymmetries of these processes are presented in Table IV. Figure 14 represents the variation of the LNU parameters ($R^{\tau\mu}_{K,\pi,\eta,\eta'}$) due to only S_R coupling. The variation of $R^{\tau}_{PP'}$ parameters is similar to those with S_L coupling. Table V contains the numerical values of these parameters.

The rare semileptonic $B_s \to Kl\bar{\nu}_l$ and $B \to \pi l\bar{\nu}_l$ processes are investigated in Refs. [16,17]. The analyses of $B \to \pi l\bar{\nu}_l$ processes using the light cone QCD sum rule

TABLE IV. Same as Table II in the presence of $S_{L,R}$ NP couplings.

Observables	Values for S_L coupling	Values for S_R coupling
$\mathrm{BR}(B_s \to K^+\mu^-\bar{\nu}_\mu)$	$(1.1 - 1.15) \times 10^{-4}$	$(1.1 - 1.15) \times 10^{-4}$
$\mathrm{BR}(B_s \to K^+\tau^-\bar{\nu}_\tau)$	$(0.62 - 1.29) \times 10^{-4}$	$(4.97 - 7.4) \times 10^{-5}$
$\langle A^\mu_{FB}\rangle$	$(-3.32 \to 3.52) \times 10^{-3}$	$(-3.32 \to 3.52) \times 10^{-3}$
$\langle A^\tau_{FB}\rangle$	0.255–0.272	0.058–0.26
$\mathrm{BR}(\bar{B} \to \pi^+\mu^-\bar{\nu}_\mu)$	$(1.39 - 1.49) \times 10^{-4}$	$(1.39 - 1.49) \times 10^{-4}$
$\mathrm{BR}(\bar{B} \to \pi^+\tau^-\bar{\nu}_\tau)$	$(0.82 - 1.93) \times 10^{-4}$	$(0.66 - 1.02) \times 10^{-4}$
$\langle A^\mu_{FB}\rangle$	$(-3.86 \to 3.51) \times 10^{-3}$	$(-3.86 \to 3.51) \times 10^{-3}$
$\langle A^\tau_{FB}\rangle$	0.25–0.27	0.0264–0.2468
$\mathrm{BR}(B^- \to \eta^0\mu^-\bar{\nu}_\mu)$	$(3.28 - 3.44) \times 10^{-5}$	$(3.28 - 3.44) \times 10^{-5}$
$\mathrm{BR}(B^- \to \eta^0\tau^-\bar{\nu}_\tau)$	$(1.74 - 3.82) \times 10^{-5}$	$(1.32 - 2.12) \times 10^{-5}$
$\langle A^\mu_{FB}\rangle$	$(-3.39 \to 4.0) \times 10^{-3}$	$(-3.39 \to 4.0) \times 10^{-3}$
$\langle A^\tau_{FB}\rangle$	0.27–0.277	0.085–0.272
$\mathrm{BR}(B^- \to \eta'^0\mu^-\bar{\nu}_\mu)$	$(1.49 - 1.55) \times 10^{-5}$	$(1.49 - 1.55) \times 10^{-5}$
$\mathrm{BR}(B^- \to \eta'^0\tau^-\bar{\nu}_\tau)$	$(0.7 - 1.46) \times 10^{-5}$	$(5.0 - 8.33) \times 10^{-6}$
$\langle A^\mu_{FB}\rangle$	$(-2.82 \to 4.68) \times 10^{-3}$	$(-2.92 \to 4.68) \times 10^{-3}$
$\langle A^\tau_{FB}\rangle$	0.287–0.31	0.153–0.298

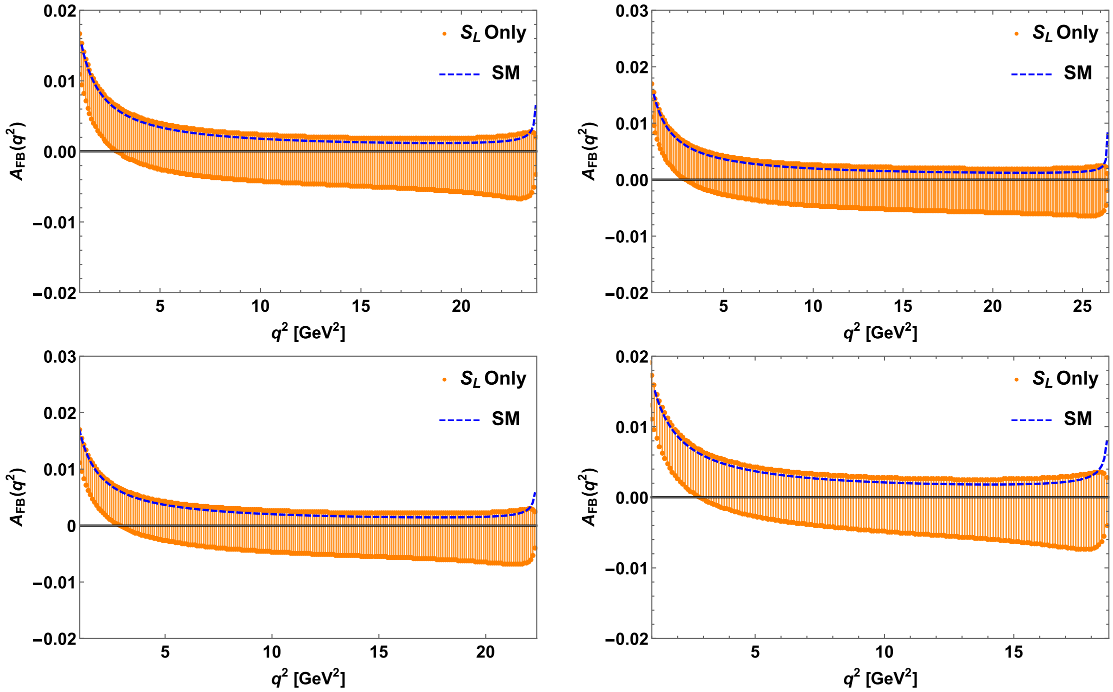

FIG. 9. The plots for the q^2 variation of forward-backward asymmetry of $\bar{B}_s \to K^+\mu^-\bar{\nu}_\mu$ (top-left panel), $\bar{B}^0 \to \pi^+\mu^-\bar{\nu}_\mu$ (top-right panel), $B^- \to \eta\mu^-\bar{\nu}_\mu$ (bottom-left panel), and $B^- \to \eta'\mu^-\bar{\nu}_\mu$ (bottom-right panel) processes.

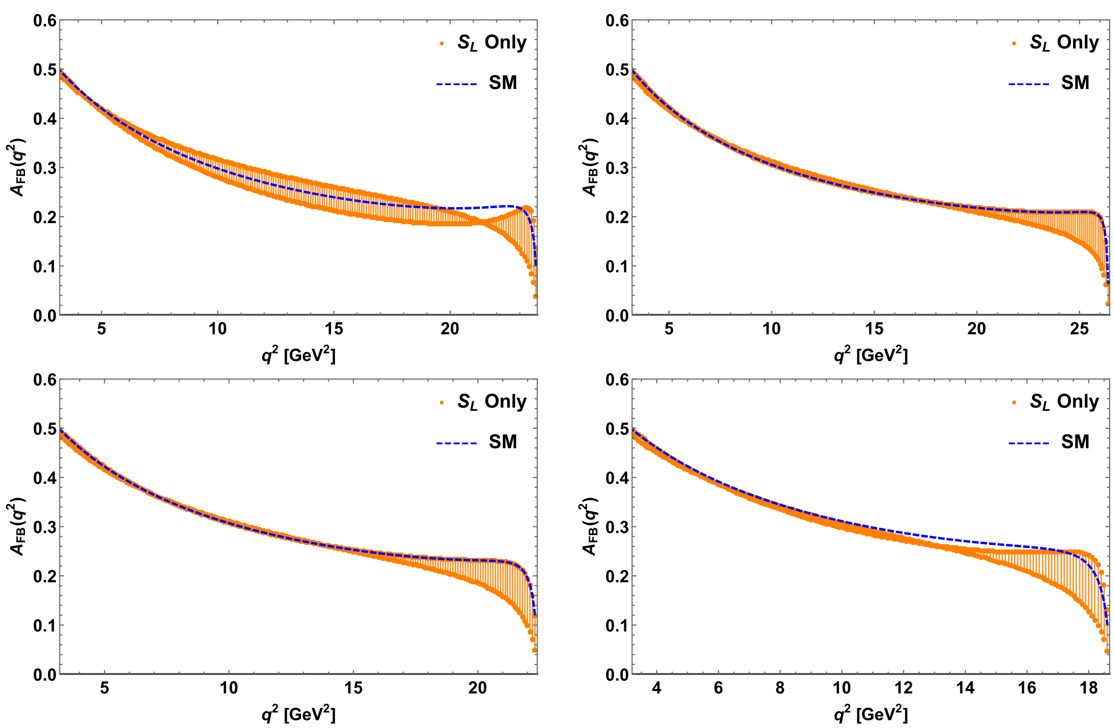

FIG. 10. The plots for the q^2 variation of forward-backward asymmetry of $\bar{B}_s \to K^+\tau^-\bar{\nu}_\tau$ (top-left panel), $\bar{B}^0 \to \pi^+\tau^-\bar{\nu}_\tau$ (top-right panel), $B^- \to \eta\tau^-\bar{\nu}_\tau$ (bottom-left panel), and $B^- \to \eta'\tau^-\bar{\nu}_\tau$ (bottom-right panel) processes.

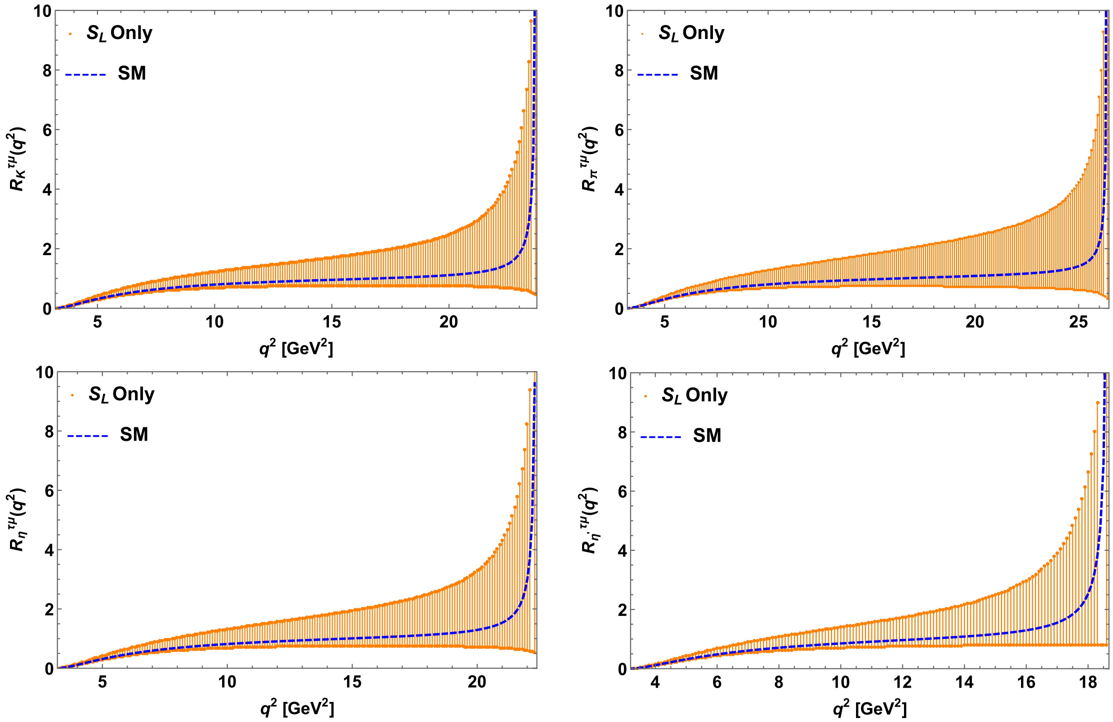

FIG. 11. The plots for the LNU parameters $R_K^{\tau\mu}(q^2)$ (top-left panel), $R_\pi^{\tau\mu}(q^2)$ (top-right panel), $R_\eta^{\tau\mu}(q^2)$ (bottom-left panel), and $R_{\eta'}^{\tau\mu}(q^2)$ (bottom-right panel) due to S_L coupling.

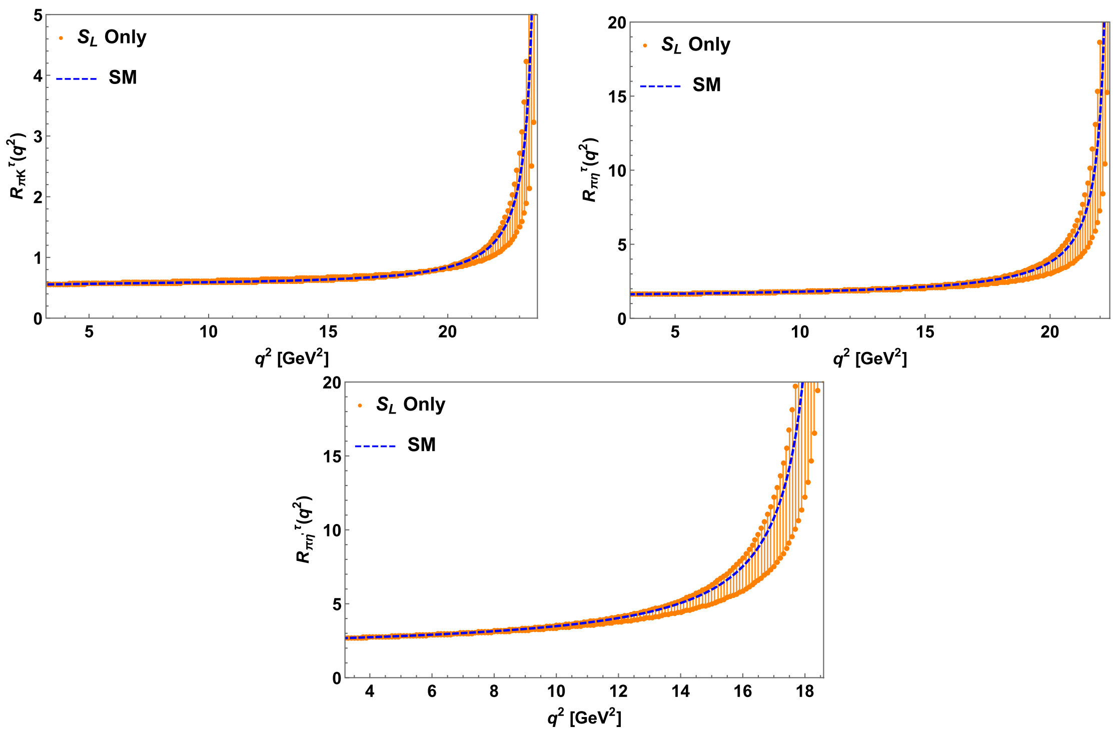

FIG. 12. The plots for $R_{\pi K}^\tau(q^2)$ (top-left panel), $R_{\pi\eta}^\tau(q^2)$ (top-right panel), and $R_{\pi\eta'}^\tau(q^2)$ (bottom panel) parameters.

TABLE V. Same as Table III in the presence of $S_{L,R}$ NP couplings.

Observables	Values for S_L coupling	Values for S_R coupling
$R_K^{\tau\mu}$	0.537–1.17	0.45–0.645
$R_\pi^{\tau\mu}$	0.55–1.38	0.47–0.685
$R_\eta^{\tau\mu}$	0.5–1.16	0.4–0.62
$R_{\eta'}^{\tau\mu}$	0.448–0.976	0.33–0.538
$R_{\pi K}^{\mu}$	1.263–1.3	1.263–1.3
$R_{\pi\eta}^{\mu}$	4.238–4.33	4.238–4.33
$R_{\pi\eta'}^{\mu}$	9.329–9.61	9.329–9.61
$R_{\pi K}^{\tau}$	1.32–1.5	1.328–1.378
$R_{\pi\eta}^{\tau}$	4.71–5.05	4.81–5.0
$R_{\pi\eta'}^{\tau}$	11.71–13.22	12.45–13.2

approach [24] and Two Higgs Doublet model [20] are also studied in the literature. In Refs. [21–23], $B \to \eta^{(\prime)} l \bar{\nu}_l$ processes are studied by using various model-dependent approaches. The model-independent analysis of $b \to u l \bar{\nu}_l$ processes can be found in Ref. [15]. Our predicted SM values of the branching ratios of $\bar{B}_{(s)} \to P^+ l^- \bar{\nu}_l$ processes are found to be consistent with the predicted results in the literature, though due to updated input parameters, the central values of the branching ratios of these processes have slight deviations.

IV. $B \to V l \bar{\nu}_l$ PROCESSES

In this section, we study the $B \to V l \bar{\nu}_l$ processes, in which $V = K^*, \rho$. The hadronic matrix element of the $B \to V l \bar{\nu}_l$ processes can be parametrized as [30]

$$\begin{aligned}
&\langle V(k,\varepsilon)|\bar{u}\gamma_\mu b|\bar{B}(p_B)\rangle \\
&\quad = -i\epsilon_{\mu\nu\rho\sigma}\varepsilon^{\nu*} p_B^\rho k^\sigma \frac{2V(q^2)}{M_B+M_V}, \\
&\langle V(k,\varepsilon)|\bar{u}\gamma_\mu\gamma_5 b|\bar{B}(p_B)\rangle \\
&\quad = \varepsilon^{\mu*}(M_B+M_V)A_1(q^2) - (p_B+k)_\mu(\varepsilon^*\cdot q)\frac{A_2(q^2)}{M_B+M_V} \\
&\qquad - q_\mu(\varepsilon^*\cdot q)\frac{2M_V}{q^2}[A_3(q^2)-A_0(q^2)],
\end{aligned} \tag{23}$$

where

$$A_3(q^2) = \frac{M_B+M_V}{2M_V}A_1(q^2) - \frac{M_B-M_V}{2M_V}A_2(q^2). \tag{24}$$

The differential decay rate of $B \to V l \nu_l$ processes with respect to q^2 is given by [30]

$$\begin{aligned}
\frac{d\Gamma(B\to V l\bar{\nu}_l)}{dq^2} = {}& \frac{G_F^2|V_{ub}|^2}{192\pi^3 M_B^3} q^2\sqrt{\lambda_V(q^2)}\left(1-\frac{m_l^2}{q^2}\right)^2 \Bigg\{(|1+V_L|^2+|V_R|^2)\left[\left(1+\frac{m_l^2}{2q^2}\right)(H_{V,+}^2+H_{V,-}^2+H_{V,0}^2)+\frac{3}{2}\frac{m_l^2}{q^2}H_{V,t}^2\right] \\
& -2\mathrm{Re}[(1+V_L)V_R^*]\left[\left(1+\frac{m_l^2}{2q^2}\right)(H_{V,0}^2+2H_{V,+}H_{V,-})+\frac{3}{2}\frac{m_l^2}{q^2}H_{V,t}^2\right] \\
& +\frac{3}{2}|S_L-S_R|^2H_S^2+3\mathrm{Re}[(1+V_L-V_R)(S_L^*-S_R^*)]\frac{m_l}{\sqrt{q^2}}H_S H_{V,t}\Bigg\},
\end{aligned} \tag{25}$$

where $\lambda_V = \lambda(M_B^2, M_V^2, q^2)$ and the hadronic amplitudes in terms of the form factors are given as

$$\begin{aligned}
H_{V,\pm}(q^2) &= (M_B+M_V)A_1(q^2) \mp \frac{\sqrt{\lambda_V(q^2)}}{M_B+M_V}V(q^2), \\
H_{V,0}(q^2) &= \frac{M_B+M_V}{2M_V\sqrt{q^2}}\left[-(M_B^2-M_V^2-q^2)A_1(q^2) \right. \\
&\qquad \left. + \frac{\lambda_V(q^2)}{(M_B+M_V)^2}A_2(q^2)\right], \\
H_{V,t}(q^2) &= -\sqrt{\frac{\lambda_V(q^2)}{q^2}}A_0(q^2), \\
H_S(q^2) &= -H_{S_2}^0(q^2) \simeq -\frac{\sqrt{\lambda_V(q^2)}}{m_b+m_u}A_0(q^2).
\end{aligned} \tag{26}$$

For the momentum transfer dependence of the form factors, we consider the most intuitive and the simplest parametrization of the $B_{(s)} \to (K^*)\rho$ form factors, ($V(q^2)$, $A_{0,1,2}(q^2)$) from Ref. [37]. The masses of all the particles are taken from Ref. [27]. Using these input values and the bounds on V_L coupling obtained from $B_u^+ \to \tau^+\nu_\tau$ and $B^- \to \pi^0\mu^-\bar{\nu}_\mu$ processes (discussed in Secs. II and III), we show the plots for the q^2 variation of branching ratios for $\bar{B}_s \to K^{*+}\mu^-\bar{\nu}_\mu$ (top-left panel) and $\bar{B}_s \to K^{*+}\tau^-\bar{\nu}_\tau$ (top-right panel) processes in the presence of V_L in Fig. 15. The corresponding plots in the bottom panel of this figure are for V_R coupling. In the presence of V_R coupling, we found reasonable deviation of the branching ratios from the SM predictions, whereas V_L affects mainly the $\bar{B}_s \to K^{*+}\tau^-\bar{\nu}_\tau$ process. In the top-left panel of Fig. 16, we show the q^2 variation of forward-backward asymmetries of

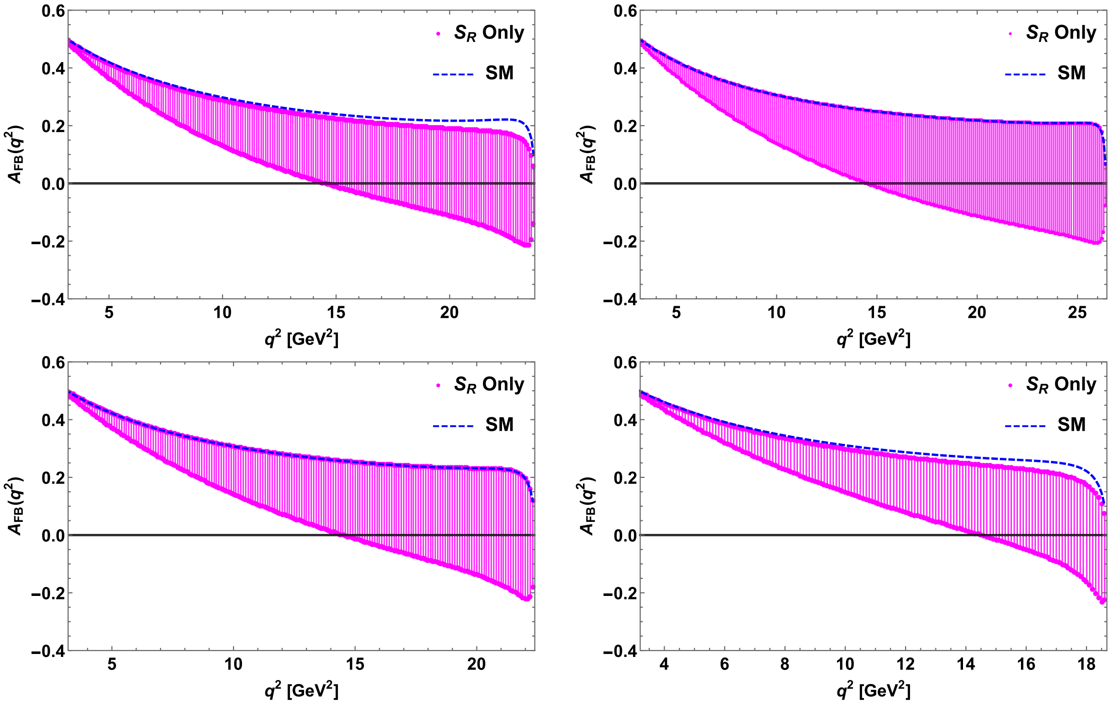

FIG. 13. The plots for the q^2 variation of forward-backward asymmetry of $\bar{B}_s \to K^+\tau^-\bar{\nu}_\tau$ (top-left panel), $\bar{B}^0 \to \pi^+\tau^-\bar{\nu}_\tau$ (top-right panel), $B^- \to \eta\tau^-\bar{\nu}_\tau$ (bottom-left panel), and $B^- \to \eta'\tau^-\bar{\nu}_\tau$ (bottom-right panel) processes.

$B_s \to K^{*+}\mu^-\bar{\nu}_\mu$ processes for V_R coupling. The forward-backward asymmetry of $B_s \to K^{*+}\tau^-\bar{\nu}_\tau$ processes for V_R (top-right panel), S_L (bottom-left panel), and S_R (bottom-right panel) couplings are presented in Fig. 16. We found significant deviation in the forward-backward asymmetry parameters from SM values due to the additional V_R and $S_{L,R}$ couplings. The presence of V_L coupling does not affect the forward-backward asymmetry parameters. As

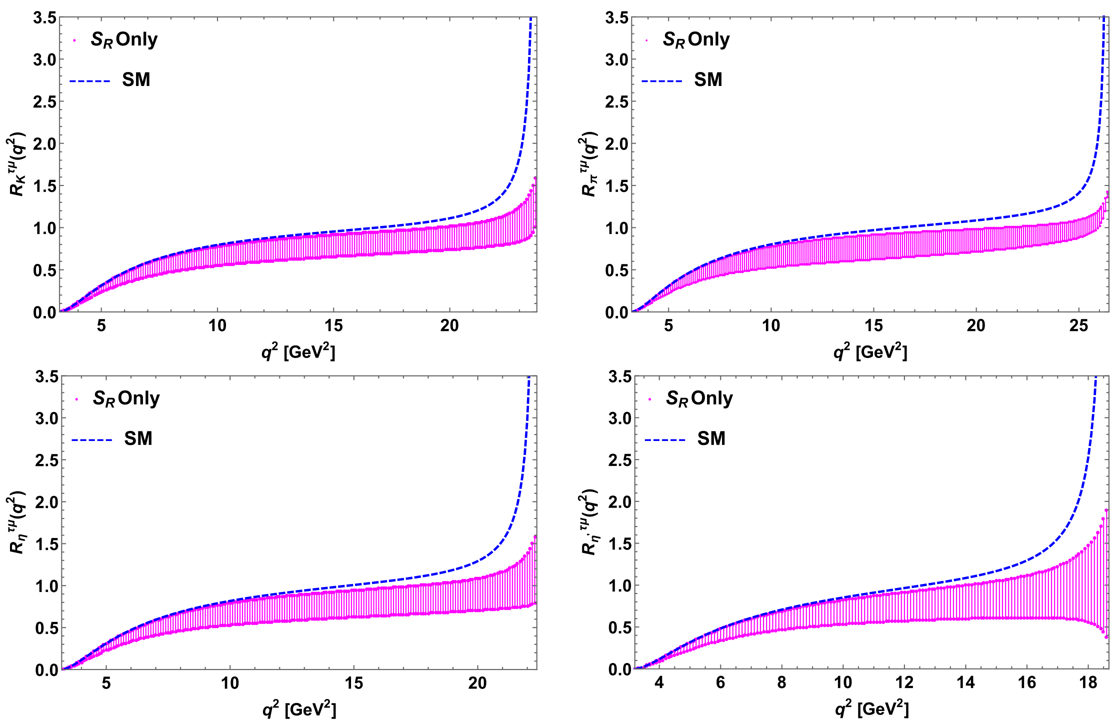

FIG. 14. The plots for the LNU parameters $R_K^{\tau\mu}(q^2)$ (top-left panel), $R_\pi^{\tau\mu}(q^2)$ (top-right panel), $R_\eta^{\tau\mu}(q^2)$ (bottom-left panel), and $R_{\eta'}^{\tau\mu}(q^2)$ (bottom-right panel) due to S_R coupling.

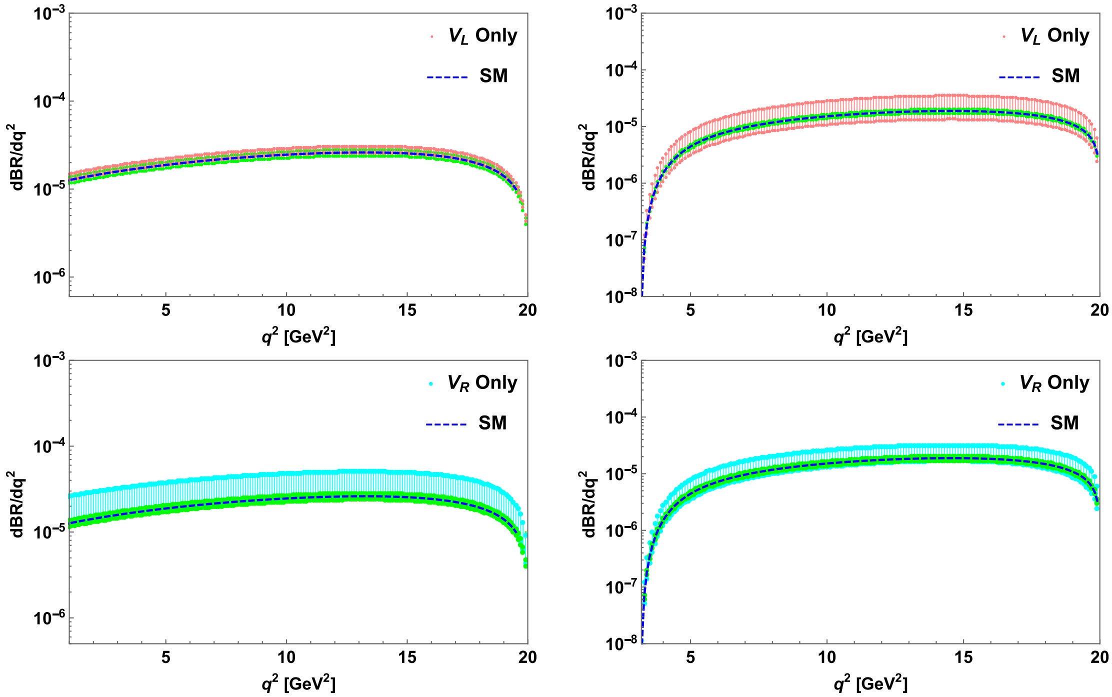

FIG. 15. The plots in the top panel represent the q^2 variation of the branching ratios of $\bar{B}_s \to K^{*+}\mu^-\bar{\nu}_\mu$ (top-left panel) and $\bar{B}_s \to K^{*+}\tau^-\bar{\nu}_\tau$ (top-right panel) processes for only V_L coupling. The corresponding plots for only V_R coupling are shown in the bottom panel.

seen from the figure, due to $S_{L,R}$ couplings, the forward-backward asymmetry of the $\bar{B}_s \to K^{*+}\tau^-\bar{\nu}_\tau$ process receives significant deviation from its SM values, whereas the deviation is negligible for the $\bar{B}_s \to K^{*+}\mu^-\bar{\nu}_\mu$ process. The integrated values of the branching ratios and the forward-backward asymmetries for $V_{L,R}$ and $S_{L,R}$ couplings are presented in Tables VI and VII, respectively. In Fig. 17, we present the plots for the $R_{K^*}^{\tau\mu}(q^2)$ parameters for V_L (top-left

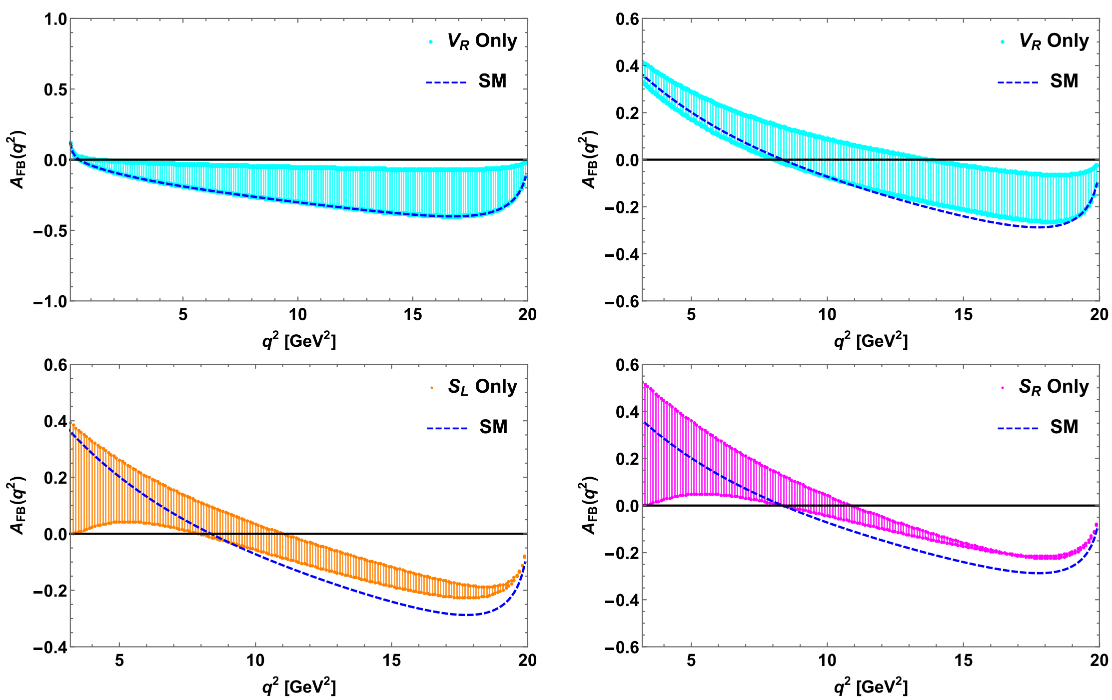

FIG. 16. The plots for the q^2 variations of the forward-backward asymmetry of $\bar{B}_s \to K^{*+}\tau^-\bar{\nu}_\tau$ processes for only V_R (top-right panel), S_L (bottom-left panel), and S_R (bottom-right panel) couplings. The top-left panel represents the plots for the forward-backward asymmetry of $\bar{B}_s \to K^{*+}\mu^-\bar{\nu}_\mu$ processes for only V_R coupling.

TABLE VI. The predicted branching ratios, forward-backward asymmetries of $\bar{B}_{(s)} \to V^+ l^- \bar{\nu}_l$ processes, in which $V = K^*, \rho$ and $l = \mu, \tau$ in the SM and for the case of $V_{L,R}$ NP couplings.

Observables	Values in the SM	Values for V_L coupling	Values for V_R coupling
$\mathrm{BR}(B_s \to K^{*+}\mu^-\bar{\nu}_\mu)$	$(3.97 \pm 0.32) \times 10^{-4}$	$(3.97 - 4.68) \times 10^{-4}$	$(3.97 - 8.05) \times 10^{-4}$
$\mathrm{BR}(B_s \to K^{*+}\tau^-\bar{\nu}_\tau)$	$(2.16 \pm 0.173) \times 10^{-4}$	$(1.54 - 4.0) \times 10^{-4}$	$(1.92 - 3.8) \times 10^{-4}$
$\langle A_{FB}^\mu \rangle$	-0.293 ± 0.023	-0.293	$-0.293 \to -0.052$
$\langle A_{FB}^\tau \rangle$	-0.146 ± 0.012	-0.146	$-0.138 \to 0.037$
$\mathrm{BR}(B^- \to \rho^0\mu^-\bar{\nu}_\mu)$	$(1.56 \pm 0.124) \times 10^{-4}$	$(1.56 - 1.85) \times 10^{-4}$	$(1.56 - 3.0) \times 10^{-4}$
$\mathrm{BR}(B^- \to \rho^0\tau^-\bar{\nu}_\tau)$	$(8.97 \pm 0.71) \times 10^{-5}$	$(0.64 - 1.67) \times 10^{-4}$	$(0.8 - 1.52) \times 10^{-4}$
$\langle A_{FB}^\mu \rangle$	-0.362 ± 0.028	-0.362	$-0.362 \to -0.065$
$\langle A_{FB}^\tau \rangle$	-0.184 ± 0.015	-0.184	$-0.168 \to 0.024$

TABLE VII. Same as in Table VI in the presence of $S_{L,R}$ couplings.

Observables	Values for S_L coupling	Values for S_R coupling
$\mathrm{BR}(B_s \to K^{*+}\mu^-\bar{\nu}_\mu)$	$(3.97 - 4.0) \times 10^{-4}$	$(3.97 - 4.0) \times 10^{-4}$
$\mathrm{BR}(B_s \to K^{*+}\tau^-\bar{\nu}_\tau)$	$(2.1 - 2.58) \times 10^{-4}$	$(1.99 - 2.2) \times 10^{-4}$
$\langle A_{FB}^\mu \rangle$	$-0.293 \to -0.291$	$-0.293 \to -0.286$
$\langle A_{FB}^\tau \rangle$	$-0.169 \to -0.043$	$-0.144 \to -0.056$
$\mathrm{BR}(B^- \to \rho^0\mu^-\bar{\nu}_\mu)$	$(1.57 - 1.6) \times 10^{-4}$	$(1.57 - 1.6) \times 10^{-4}$
$\mathrm{BR}(B^- \to \rho^0\tau^-\bar{\nu}_\tau)$	$(0.87 - 1.12) \times 10^{-4}$	$(8 - 9.2) \times 10^{-5}$
$\langle A_{FB}^\mu \rangle$	$-0.36 \to -0.35$	$-0.36 \to -0.35$
$\langle A_{FB}^\tau \rangle$	$-0.21 \to -0.07$	$-0.32 \to -0.18$

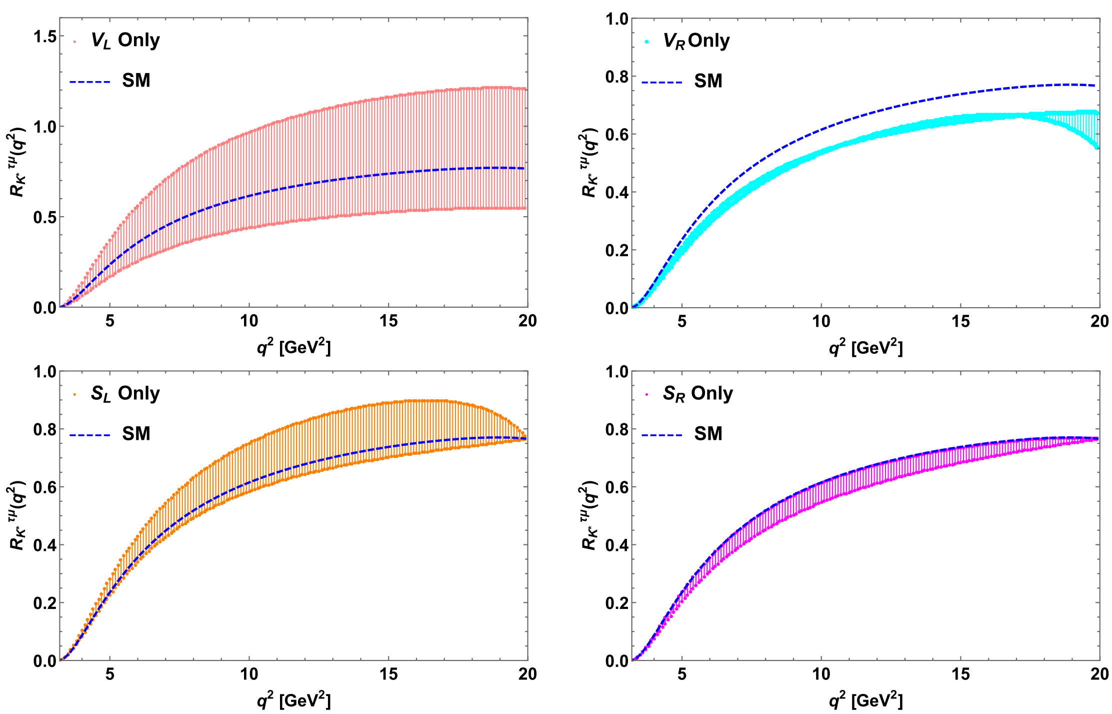

FIG. 17. The plots for $R_{K^*}^{\tau\mu}(q^2)$ parameters versus q^2 for only V_L (top-left panel), V_R (top-right panel), S_L (bottom-left panel), and S_R (bottom-right panel) couplings.

TABLE VIII. Values of $R_{K^*}^{\tau\mu}$, $R_{\rho}^{\tau\mu}$, $R_{\rho K^*}^{\mu}$, and $R_{\rho K^*}^{\tau}$ parameters for different cases of NP couplings.

Model	$R_{K^*}^{\tau\mu}$	$R_{\rho}^{\tau\mu}$	$R_{\rho K^*}^{\mu}$	$R_{\rho K^*}^{\tau}$
SM	0.544	0.573	0.393	0.415
V_L	0.388–0.856	0.41–0.9	0.393–0.395	0.415–0.42
V_R	0.47–0.474	0.5–0.51	0.373–0.393	0.4–0.42
S_L	0.522–0.646	0.542–0.712	0.393–0.4	0.414–0.434
S_R	0.497–0.544	0.5–0.573	0.393–0.4	0.4–0.42

panel), V_R (top-right panel), S_L (bottom-left panel), and S_R (bottom-right panel) couplings, and the corresponding integrated values are presented in Table VIII.

The q^2 variation of the branching ratios of $\bar{B} \to \rho^+ l^- \bar{\nu}_l$ processes for $V_{L,R}$ couplings are presented in Fig. 18. In the presence of $S_{L,R}$ couplings, the branching ratios of $\bar{B} \to \rho^+ l^- \bar{\nu}_l$ processes have negligible deviation from the SM predictions. The predicted values of the branching ratios of these processes are given in Tables VI and VII, respectively. The experimental branching ratio of the $B^+ \to \rho^0 l^+ \nu_l$ process is [27]

$$\mathrm{BR}(B^+ \to \rho^0 l^+ \nu_l)^{\mathrm{Expt}} = (1.58 \pm 0.11) \times 10^{-4}. \quad (27)$$

Our predicted results for the $B^- \to \rho^0 \mu^- \bar{\nu}_\mu$ process is consistent with the above experimental data (though a part of the allowed parameter space of $V_{L,R}$ and $S_{L,R}$ gives values on the higher side of the observed central value). The forward-backward asymmetry plots for $\bar{B} \to \rho^+ l^- \bar{\nu}_l$ are presented in Fig. 19, and the corresponding numerical values are given in Tables VI and VII. Figure 20 represents the plots of the LNU parameter $R_{\rho}^{\tau\mu}(q^2)$ for V_L (top-left panel), V_R (top-right panel), S_L (bottom-left panel), and S_R (bottom-right panel) couplings. In Fig. 21, we show the variation of the parameter $R_{\rho K^*}^{\tau}(q^2)$ with respect to q^2 for only S_L (left panel) and S_R (right panel) couplings. The integrated values of these parameters are given in Table VIII. The additional $V_{L,R}$ couplings do not affect the $R_{\rho K^*}^{l}$ parameters.

In the literature, the $B \to V l \nu_l$ processes are investigated in both model-dependent and -independent ways [15,19]. Our findings on these processes are consistent with these predictions.

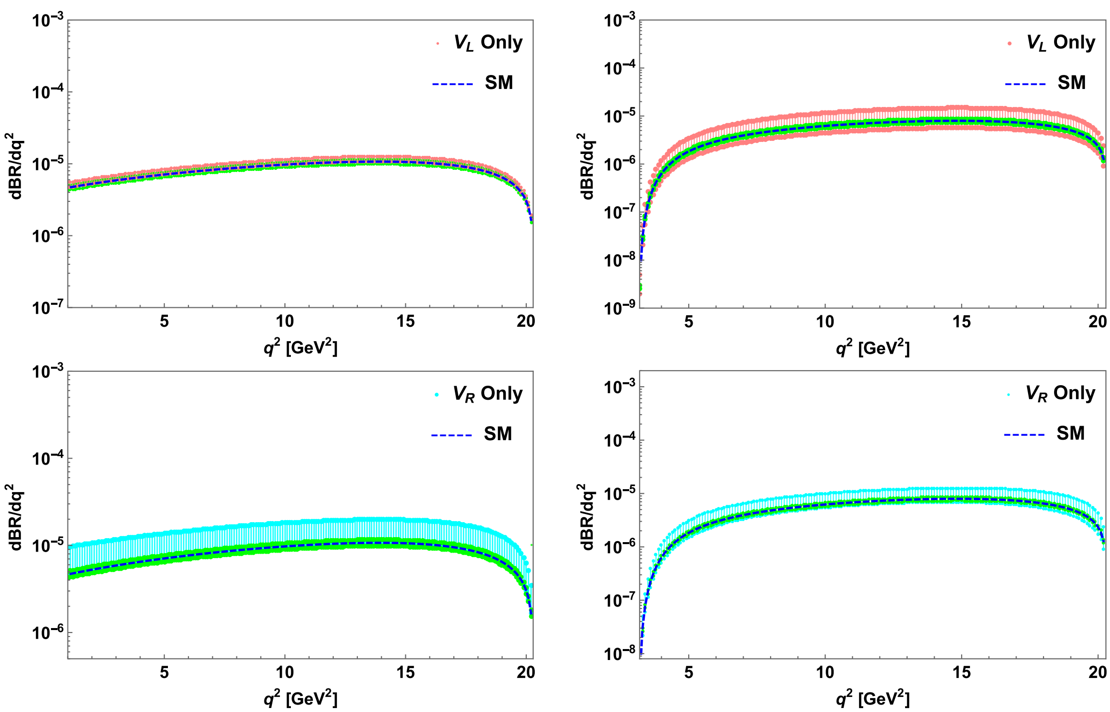

FIG. 18. Same as Fig. 15 for $B^- \to \rho^0 l^- \bar{\nu}_l$ processes.

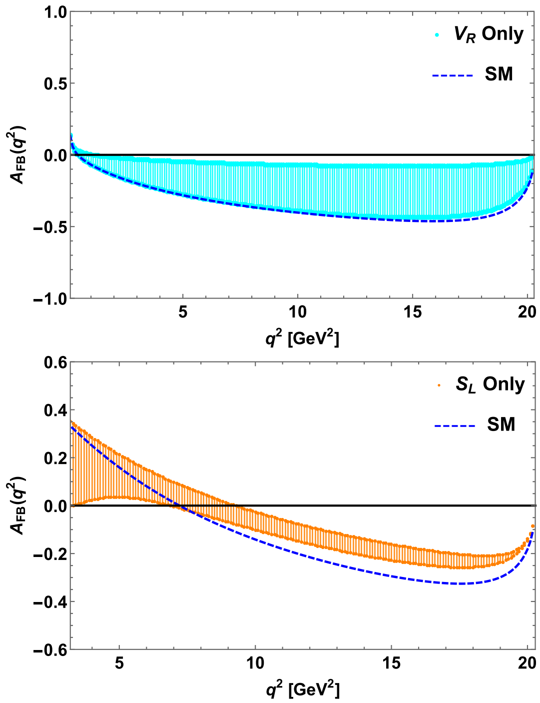

FIG. 19. Same as Fig. 16 for $B^- \to \rho^0 l^- \bar{\nu}_l$ processes.

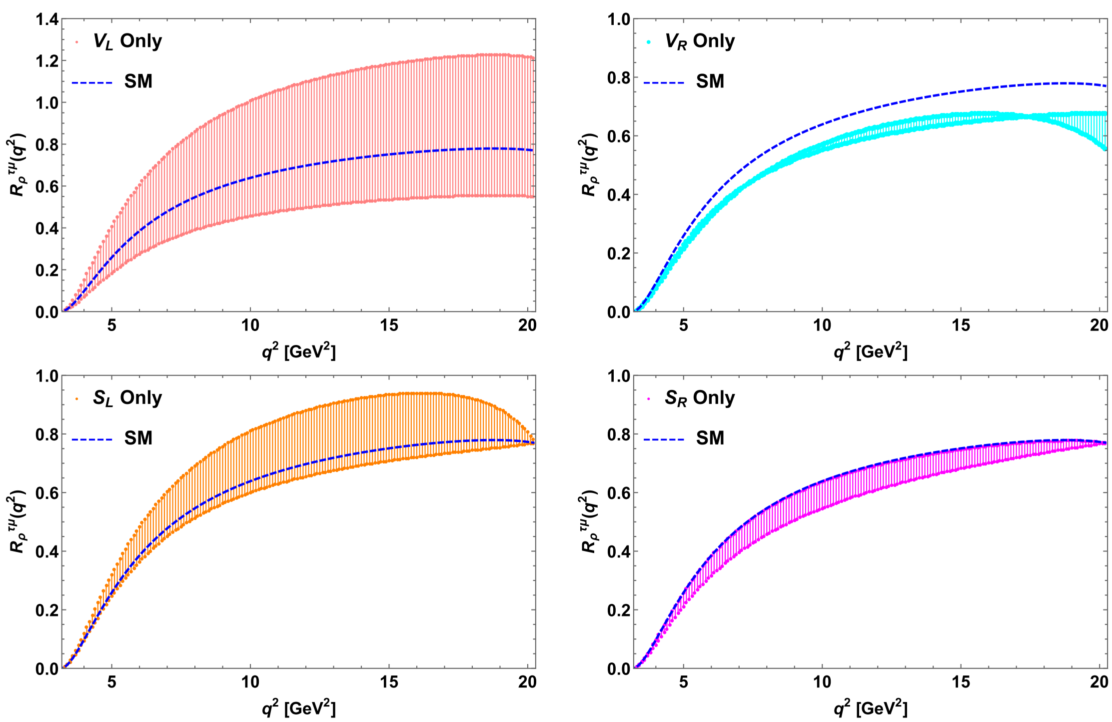

FIG. 20. Same as Fig. 17 for $B^- \to \rho^0 l^- \bar{\nu}_l$ processes.

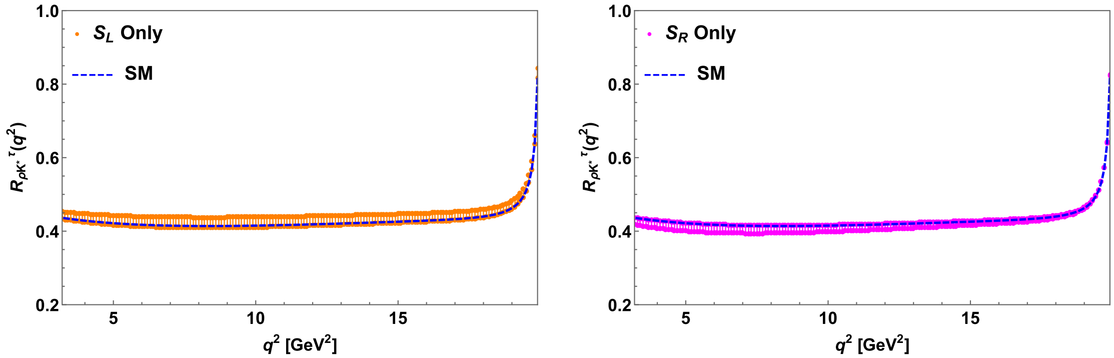

FIG. 21. The plots for $R^\tau_{\rho K^*}(q^2)$ parameters versus q^2 for only S_L (left panel) and S_R (right panel) couplings.

V. CONCLUSION

Inspired by the recent measurement of the $R_{K^{(*)}}$ parameter at LHCb and the observed $R_{D^{(*)}}$ anomalies in $b \to sl^+l^-$ and $b \to cl\bar{\nu}_l$ processes, we performed a model-independent analysis of the rare semileptonic $b \to ul\bar{\nu}_l$ processes in this paper. We considered the generalized effective Lagrangian in the presence of new physics, which contributes additional coefficients to the SM. In our work, the new coefficients are considered to be complex, and we took into account the effect of one Wilson coefficient at a time to compute the allowed parameter space of these new coefficients. Using the experimental branching ratios of $B_u^+ \to \tau^+\nu_\tau$ and $B^- \to \pi^0\mu^-\bar{\nu}_\mu$ processes, we constrained the new couplings. We then calculated the branching ratios, forward-backward asymmetries and lepton nonuniversality parameters of $B \to Pl\bar{\nu}_l$ processes, in which $P = K, \pi, \eta^{(\prime)}$ for all possible cases of new couplings. In the presence of $V_{L,R}$ couplings, we found reasonable deviation in the branching ratios of these processes from the corresponding SM predictions, but the corresponding forward-backward asymmetry parameters do not show any deviation. In the case of $S_{L,R}$ couplings, the branching ratios have a slight deviation from the SM predictions. However, the forward-backward asymmetry parameters have comparatively large deviations from the SM values. We then computed the lepton nonuniversality parameters, in order to test the presence of the violation of lepton universality in $b \to ul\bar{\nu}_l$ processes.

Besides the semileptonic decays of a B meson to a pseudoscalar meson, we also studied the $B \to Vl\bar{\nu}_l$ processes, in which V is a vector meson and $V = K^*, \rho$. We calculated the branching ratios, forward-backward asymmetries, and the lepton nonuniversality parameters for these processes. The presence of additional $V_{L,R}$ Wilson coefficients results in a larger deviation in the branching ratios and other observables in the $B \to Vl\bar{\nu}_l$ processes. The effect of $S_{L,R}$ couplings on branching ratios of these processes is almost negligible. However, the forward-backward asymmetry of the $B \to V\tau\bar{\nu}_\tau$ process deviates significantly from the SM. We also observed that the rare semileptonic $b \to ul\bar{\nu}_l$ processes also violate the lepton flavor universality. Thus, the study of $b \to ul\bar{\nu}_l$ processes is necessary in both theoretical and experimental points of view in order to search new physics.

ACKNOWLEDGMENTS

S. S. and R. M. would like to thank Science and Engineering Research Board (SERB), Government of India, for financial support through Grant No. SB/S2/HEP-017/2013. A. R. acknowledges University Grants Commission for financial support.

[1] R. Aaij *et al.* (LHCb Collaboration), Phys. Rev. Lett. **111**, 191801 (2013).
[2] S. Descotes-Genon, J. Matias, M. Ramon, and J. Virto, J. High Energy Phys. 01 (2013) 048.
[3] R. Aaij *et al.* (LHCb Collaboration), J. High Energy Phys. 06 (2014) 133.
[4] R. Aaij *et al.* (LHCb Collaboration), J. High Energy Phys. 07 (2013) 084.
[5] R. Aaij *et al.* (LHCb Collaboration), Phys. Rev. Lett. **113**, 151601 (2014).
[6] C. Bobeth, G. Hiller, and G. Piranishvili, J. High Energy Phys. 12 (2007) 040.
[7] R. Aaij *et al.* (LHCb Collaboration), J. High Energy Phys. 08 (2017) 055.
[8] B. Capdevila, A. Crivellin, S. Descotes-Genon, J. Matias, and J. Virto, arXiv:1704.05340.

[9] J. Lees *et al.* (*BABAR* Collaboration), Phys. Rev. Lett. **109**, 101802 (2012); Phys. Rev. D **88**, 072012 (2013); M. Huschle *et al.* (Belle Collaboration), Phys. Rev. D **92**, 072014 (2015); A. Abdesselam *et al.* (Belle Collaboration), arXiv:1603.06711.
[10] Heavy Flavour Averaging Group Collaboration, http://www.slac.stanford.edu/xorg/hfag/semi/winter16/winter16_dtaunu.html.
[11] R. Aaij *et al.* (LHCb Collaboration), Phys. Rev. Lett. **115**, 111803 (2015); **115**, 159901(A) (2015).
[12] H. Na, C. M. Bouchard, G. P. Lepage, C. Monahan, and J. Shigemitsu, Phys. Rev. D **92**, 054510 (2015).
[13] S. Fajfer, J. F. Kamenik, and I. Nisandzic, Phys. Rev. D **85**, 094025 (2012); S. Fajfer, J. F. Kamenik, I. Nisandzic, and J. Zupan, Phys. Rev. Lett. **109**, 161801 (2012).
[14] C. Bourrely, I. Caprini, and L. Lellouch, Phys. Rev. D **79**, 013008 (2009); **82**, 099902(E) (2010); F. U. Bernlochner, Z. Ligeti, and S. Turczyk, Phys. Rev. D **90**, 094003 (2014).
[15] R. Dutta, A. Bhol, and A. K. Giri, Phys. Rev. D **88**, 114023 (2013); R. Dutta and A. Bhol, Phys. Rev. D **96**, 036012 (2017).
[16] J. M. Flynn, T. Izubuchi, T. Kawanai, C. Lehner, A. Soni, R. S. V. de Water, and O. Witzel, Phys. Rev. D **91**, 074510 (2015).
[17] W.-F. Wang and Z.-J. Xiao, Phys. Rev. D **86**, 114025 (2012).
[18] U.-G. Meßiner and W. Wang, J. High Energy Phys. 01 (2014) 107.
[19] T. Feldmann, B. Mller, and D. van Dyk, Phys. Rev. D **92**, 034013 (2015).
[20] F. U. Bernlochner, Phys. Rev. D **92**, 115019 (2015).
[21] C. S. Kim, S. Oh, and C. Yu, Phys. Lett. B **590**, 223 (2004).
[22] T. M. Aliev, I. Kanik, and A. Ozpineci, Phys. Rev. D **67**, 094009 (2003).
[23] C. S. Kim and Y.-D. Yang, Phys. Rev. D **65**, 017501 (2001).
[24] A. Khodjamirian, R. Rükl, S. Weinzierl, C. W. Winhart, and O. Yakovlev, Phys. Rev. D **62**, 114002 (2000).
[25] T. Bhattacharya, V. Cirigliano, S. D. Cohen, A. Filipuzzi, M. Gonzalez-Alonso, M. L. Graesser, R. Gupta, and H.-W. Lin, Phys. Rev. D **85**, 054512 (2012); V. Cirigliano, J. Jenkins, and M. Gonzalez-Alonso, Nucl. Phys. **B830**, 95 (2010).
[26] P. Biancofiore, P. Colangelo, and F. De Fazio, Phys. Rev. D **87**, 074010 (2013).
[27] C. Patrignani *et al.* (Particle Data Group Collaboration), Chin. Phys. C **40**, 100001 (2016).
[28] S. Aoki *et al.*, Eur. Phys. J. C **74**, 2890 (2014).
[29] M. Beneke and T. Feldmann, Nucl. Phys. **B592**, 3 (2001).
[30] Y. Sakaki, R. Watanabe, M. Tanaka, and A. Tayduganov, Phys. Rev. D **88**, 094012 (2013).
[31] Y.-Y. Keum, H.-N. Li, and A. I. Sanda, Phys. Lett. B **504**, 6 (2001); Phys. Rev. D **63**, 054008 (2001); C.-D. Lu, K. Ukai, and M.-Z. Yang, Phys. Rev. D **63**, 074009 (2001); C.-D. Lu and M.-Z. Yang, Eur. Phys. J. C **23**, 275 (2002).
[32] H.-N. Li, Y.-L. Shen, and Y.-M. Wang, Phys. Rev. D **85**, 074004 (2012).
[33] A. Khodjamirian, T. Mannel, N. Offen, and Y.-M. Wang, Phys. Rev. D **83**, 094031 (2011).
[34] C. Bourrely, I. Caprini, and L. Lellouch, Phys. Rev. D **79**, 013008 (2009); C. G. Boyd, B. Grinstein, and R. F. Lebed, Phys. Rev. Lett. **74**, 4603 (1995); Phys. Lett. B **353**, 306 (1995).
[35] J. L. Rosner, Phys. Rev. D **27**, 1101 (1983); A. Bramon, R. Escribano, and M. D. Scadron, Eur. Phys. J. C **7**, 271 (1998).
[36] T. Feldmann, P. Kroll, and B. Stech, Phys. Rev. D **58**, 114006 (1998); Phys. Lett. B **449**, 339 (1999); T. Feldmann, Int. J. Mod. Phys. A **15**, 159 (2000).
[37] P. Ball and R. Zwicky, Phys. Rev. D **71**, 014029 (2005).